**Numerische Mathematik manuscript No.**
(will be inserted by the editor)

# Finite element analysis of the nearly incompressible linear elasticity eigenvalue problem with variable coefficients

**Arbaz Khan · Felipe Lepe · David Mora · Jesus Vellojin**

Received: date / Revised version: date Updated: December 17, 2023

**Abstract** In this paper we present a mathematical and numerical analysis of an eigenvalue problem associated to the elasticity-Stokes equations stated in two and three dimensions. Both problems are related through the Herrmann pressure. Employing the Babuška–Brezzi theory, it is proved that the resulting continuous and discrete variational formulations are well-posed. In particular, the finite element method is based on general inf-sup stables pairs for the Stokes system, such that, Taylor–Hood finite elements. By using a general approximation theory for compact operators, we obtain optimal order error estimates for the eigenfunctions and a double order for the eigenvalues. Under mild assumptions, we have that these estimates hold with constants independent of the Lamé coefficient $\lambda$. In addition, we carry out the reliability and efficiency analysis of a residual-based a posteriori error estimator for the spectral problem. We report a series of numerical tests in order to assess the performance of the method and its behavior when the nearly incompressible case of elasticity is considered.

**Keywords** elasticity eigenvalue problem · Stokes eigenvalue problem · finite elements · a priori error estimates · a posteriori error bounds

**Mathematics Subject Classification (2000)** 65N30 · 65N12 · 76D07 · 65N15

## 1 Introduction

The accurate solution of eigenvalue problems coming from continuum mechanics is crucial because the stability of systems relying on fluids or structures, or their coupling, hinges on understanding vibration modes associated with spectral problems. Notable monographs currently addressing this subject are cited here for reference [7].

One important aspect that is still under investigation is understanding the eigenvalue properties in parameter limits between Stokes and elasticity equations. It is well-established that in elasticity

F. Lepe · D. Mora · J. Vellojin
GIMNAP, Departamento de Matemática, Facultad de Ciencias,
Universidad del Bío-Bío, Casilla 5-C, Concepción, Chile.
E-mail: {flepe,dmora,jvellojin}@ubiobio.cl

D. Mora
CI$^2$MA, Universidad de Concepción, Casilla 160-C, Concepción, Chile.

A. Khan
Department of Mathematics, Indian Institute of Technology Roorkee, Roorkee 247667, India.
E-mail: arbaz@ma.iitr.ac.in

equations where the Poisson ratio is close to 1/2, classical numerical methods exhibit the locking phenomenon, which can be mitigated, for example, with mixed formulations, least-squares, among others (see, e.g. [13,22,21,20,5,3,14]). In this incompressible regime, the equations align with Stokes equations. A study in [16] demonstrates that the spectrum of the elasticity eigenvalue problem converges to that of the Stokes eigenvalue problem as the Poisson ratio tends to 1/2. Recent research, as seen in [24], proposes a mixed method for the linear elasticity where the stress, rotations, and displacement are considered as unknowns. Here the convergence of the method also works correctly for the case when Poisson ratio tends to 1/2. Also, novel strategies like least squares formulations have been applied to elasticity eigenvalue problems [5].

In the realm of a posteriori analysis for elasticity eigenvalue problems, we have, for example, [14], where a locking-free mixed formulation based on the finite element method has been proposed for the load problem, accompanied by a priori and a posteriori error estimates. The authors provide estimation strategies that prove to be robust with respect to the material parameters. They ensure robustness in elasticity, which involves multiple parameters compared to the single viscosity parameter in the Stokes problem. We have also the work of [6]. Here, the authors aim to expand the results obtained in a previous study of a conforming mixed finite elements for the elasticity problem to address the related eigenvalue problem. Their study shows that using a residual-type error estimator can effectively steer an adaptive scheme Additionally, they explore how implementing a postprocessing technique can improve the convergence rate of the scheme. Postprocessing techniques have also been explored recently in [18], where a reliable and efficient a posteriori error estimators for mixed formulations for the elasticity eigenvalue problem is studied, including an analysis for the perfectly incompressible case.

The concepts presented in [14] can be extended to the eigenvalue problem under the same norm. It is well-known that such a problem lacks a unique solution due to eigenvalues/eigenfunctions exhibiting a multiplicity greater than one. Adding to this, we have a parameter dependent problem that connects the elasticity eigenvalue problem with the Stokes one, where the Poisson ratio serves as the involved parameter. This is an important issue, since according this parameter changes, the spectrum of the elasticity operator changes and hence, the multiplicity of the eigenvalues starts to behave different according to this. Since we have a fixed eigenvalue problem (Stokes) as a limit, the elasticity eigenvalue problem change its spectrum according to the change of the Poisson ratio when we are approximating to the spectrum of Stokes. Then, the question that emerge is how does the spectrum of the parameter-dependent elasticity problem converge towards the Stokes spectrum. This issue is difficult to handle and must be studied.

Our contribution focuses on analyzing both the Stokes and elasticity eigenproblems within a unified locking-free system. The key lies in considering the Herrmann pressure that connects the fluid and elastic representations. The introduction of variable coefficients, reflecting the physical attributes of the structure, adds another layer of complexity to our analysis. Specifically, these variable coefficients demands the use of a weighted norm with spatial-dependent parameters in order to ensure robustness of the estimates. It is worth emphasizing that, to the best of the authors' knowledge, this work represents a pioneering effort in examining the elasticity/Stokes eigenvalue problem with variable coefficients. We also propose a scheme that expand the numerical analysis to encompass two families of finite elements known for their inf-sup stability: the Taylor-Hood elements and the mini element. Moreover, others inf-sup stable finite elements could be also considered. However, for an accurate analysis of the eigenvalue problem, certain adjustments become essential. More precisely, a suitable scaling of the problem with respect to physical parameters is required in order to achieve robustness for the spectral problem. The approach is to leverage simple tools for the analysis, and a key argument is the problem's regularity, which we will use to conduct both a priori and a posteriori error estimation with the aid of the compact operators theory [4]. Finally, we stress that our locking-free method is very competitive in terms of computational cost.

The outline of our manuscript is the following: In Section 2 we present the model problem, describing the parameters involved on the elasticity eigensystem and their relation with the Stokes eigenvalue problem through the Herrmann's pressure. We outline the scaling of the problem and the respective variational formulation which we analyze under a suitable weighted norm. Regularity results are pre-

sented together with the parameter dependent solution operator. Also, we report an analysis of the relation between the spectrums of the elasticity and the Stokes eigenvalue problems when the Poisson ratio tends to 1/2. Section 3 is dedicated to the discretization of the eigenvalue problem, where we introduce the finite element spaces for our study, the corresponding discrete version of the nearly incompressible eigenvalue problem, and we derive convergence of the method, and error estimates for the eigenvalues and eigenfunctions. In Section 4 we design an a posteriori error estimator which we prove under standard techniques it reliability and efficiency. Finally in Section 5 we report a series of numerical tests in order to study the performance of the method in two and three dimensions. Here the aims are two: first, to confirm the results related to the a priori analysis, where we compute the spectrum and order of convergence for the approximation and secondly, to analyze the performance of the a posteriori estimator where the aim is to recover the optimal order of convergence when the configuration of the problem does not allow sufficiently smooth eigenfunctions, deteriorating the a priori convergence rates.

## 2 The model problem

In this section we present the eigenvalue problem of our interest. Let $\Omega \subset \mathbb{R}^d$ with $d \in \{2, 3\}$ an open and bounded domain with Lipschitz boundary $\partial\Omega$. Let us assume that the boundary is divided into two parts $\partial\Omega := \Gamma_D \cup \Gamma_N$, where $|\Gamma_D| > 0$. In particular, we assume that the structure is fixed on $\Gamma_D$ and free of stress on $\Gamma_N$.

The eigenvalue problem of interest is given by: Find $(\widehat{\kappa}, \boldsymbol{u})$ such that

$$\begin{aligned} -\,\mathbf{div}\left[2\widehat{\mu}\boldsymbol{\varepsilon}(\boldsymbol{u}) + \widehat{\lambda}\,\mathrm{tr}(\boldsymbol{\varepsilon}(\boldsymbol{u}))\mathbb{I}\right] &= \widehat{\kappa}\rho\boldsymbol{u} \qquad \text{in } \Omega, \\ \boldsymbol{u} &= \mathbf{0} \qquad \text{on } \Gamma_D, \\ \boldsymbol{\sigma}\boldsymbol{n} &= \mathbf{0} \qquad \text{on } \Gamma_N, \end{aligned} \tag{2.1}$$

where $\sqrt{\widehat{\kappa}}$ is the natural frequency, $\boldsymbol{u}$ is the displacement, $\rho$ is the material density, the Lamé parameters $\widehat{\lambda}$ and $\widehat{\mu}$ are defined by

$$\widehat{\lambda} := \frac{E(x)\nu}{(1+\nu)(1-2\nu)} \quad \text{and} \quad \widehat{\mu} := \frac{E(x)}{2(1+\nu)},$$

and $\boldsymbol{\varepsilon}(\cdot)$ represents the strain tensor given by $\boldsymbol{\varepsilon}(\boldsymbol{v}) := \frac{1}{2}(\nabla\boldsymbol{v} + (\nabla\boldsymbol{v})^{\mathtt{t}})$ where $\mathtt{t}$ represents the transpose operator. On the other hand, regarding to the physical parameters, $E(x)$ represents the space-variable Young modulus and $\nu$ represents the Poisson ratio which we assume as a constant. Let us assume the existence of two positive constants $E_{\min}$ and $E_{\max}$ such that the Young's modulus is bounded in the sense $E_{\min} \leq E(x) \leq E_{\max}$. Scaling the first equation of (2.1) by $(1+\nu)$ we obtain the following eigenvalue problem: Find $(\kappa, \boldsymbol{u})$ such that

$$\begin{aligned} -\,\mathbf{div}\left[2\mu\boldsymbol{\varepsilon}(\boldsymbol{u}) + \lambda\,\mathrm{tr}(\boldsymbol{\varepsilon}(\boldsymbol{u}))\mathbb{I}\right] &= \kappa\rho\boldsymbol{u} \qquad \text{in } \Omega, \\ \boldsymbol{u} &= \mathbf{0} \qquad \text{on } \Gamma_D, \\ \boldsymbol{\sigma}\boldsymbol{n} &= \mathbf{0} \qquad \text{on } \Gamma_N, \end{aligned} \tag{2.2}$$

where the scaled eigenvalue and the Lamé coefficients are given by

$$\kappa := (1+\nu)\widehat{\kappa}, \qquad \lambda := \frac{E(x)\nu}{1-2\nu}, \qquad \mu := \frac{E(x)}{2}. \tag{2.3}$$

Note that for a given $E(x)$, the eigenvalue problem (2.2) has the advantage of having $\mu$ independent of $\nu$. The incompressibility of the material is explicitly given only by the behavior of the constant $\nu$ through the Lamé parameter $\lambda$.

With the scaled parameters specified in (2.3) we rewrite system (2.1) as the following system: We seek the eigenvalue $\kappa$, a vector field $\boldsymbol{u}$, and a scalar field $p$ such that

$$\begin{aligned} -\mathbf{div}(2\mu\boldsymbol{\varepsilon}(\boldsymbol{u})) + \nabla p &= \kappa\rho\boldsymbol{u} && \text{in } \Omega, \\ \operatorname{div}\boldsymbol{u} + \frac{1}{\lambda}p &= 0 && \text{in } \Omega, \\ \boldsymbol{u} &= \mathbf{0} && \text{on } \Gamma_D, \\ \boldsymbol{\sigma}\boldsymbol{n} &= \mathbf{0} && \text{on } \Gamma_N. \end{aligned} \tag{2.4}$$

We note from (2.3) that if the Poisson ratio approaches $1/2$, then $\lambda \uparrow \infty$. In such case, we recover the Stokes system. This is an important matter in view of deriving robust stability and error bounds. From now and on, and for simplicity, in the analysis below we consider $\rho = 1$.

## 2.1 Variational formulation and preliminary results

The aim of this section is to introduce a variational formulation for system (2.4). From now and on the relation $\mathtt{a} \lesssim \mathtt{b}$ indicates that $\mathtt{a} \leq C\mathtt{b}$, with a positive constant $C$ which is independent of $\mathtt{a}$, $\mathtt{b}$.

Since we are focused in the pressure and displacement, the resulting formulation is a saddle-point problem that can be studied according to the theory of Babuška–Brezzi [8].

Let us begin by defining the spaces $\mathrm{H} := \left\{\boldsymbol{v} \in \mathrm{H}^1(\Omega)^d \,:\, \boldsymbol{v} = \mathbf{0} \text{ on } \Gamma_D\right\}$ and $\mathrm{Q} := \mathrm{L}^2(\Omega)$ where we will seek the displacement and the pressure, respectively. Now, by testing system (2.4) with adequate functions and imposing the boundary conditions, we end up with the following saddle point variational formulation: Find $(\kappa, (\boldsymbol{u}, p)) \in \mathbb{R} \times \mathrm{H} \times \mathrm{Q}$ with $(\boldsymbol{u}, p) \neq (\mathbf{0}, 0)$ such that

$$\begin{aligned} 2\int_\Omega \mu(x)\boldsymbol{\varepsilon}(\boldsymbol{u}) : \boldsymbol{\varepsilon}(\boldsymbol{v})\, dx - \int_\Omega p \operatorname{div}\boldsymbol{v}\, dx &= \kappa \int_\Omega \boldsymbol{u}\cdot\boldsymbol{v}\, dx && \forall \boldsymbol{v} \in \mathrm{H}, \\ -\int_\Omega q \operatorname{div}\boldsymbol{u}\, dx - \int_\Omega \frac{1}{\lambda(x)} pq\, dx &= 0 && \forall q \in \mathrm{Q}. \end{aligned}$$

This variational problem can be rewritten as follows: *Find* $(\kappa, (\boldsymbol{u}, p)) \in \mathbb{R} \times \mathrm{H} \times \mathrm{Q}$ *such that*

$$\begin{cases} a(\boldsymbol{u}, \boldsymbol{v}) + b(\boldsymbol{v}, p) = \kappa d(\boldsymbol{u}, \boldsymbol{v}) & \forall \boldsymbol{v} \in \mathrm{H}, \\ b(\boldsymbol{u}, q) - c(p, q) = 0 & \forall q \in \mathrm{Q}, \end{cases} \tag{2.5}$$

where the bilinear forms $a : \mathrm{H} \times \mathrm{H} \to \mathbb{R}$, $b : \mathrm{H} \times \mathrm{Q} \to \mathbb{R}$, $c : \mathrm{Q} \times \mathrm{Q} \to \mathbb{R}$, and $d : \mathrm{H} \times \mathrm{H} \to \mathbb{R}$ are defined by

$$\begin{aligned} a(\boldsymbol{u}, \boldsymbol{v}) &:= 2\int_\Omega \mu(x)\boldsymbol{\varepsilon}(\boldsymbol{u}) : \boldsymbol{\varepsilon}(\boldsymbol{v})\, dx, \quad b(\boldsymbol{v}, q) := -\int_\Omega q \operatorname{div}\boldsymbol{v}\, dx, \\ d(\boldsymbol{u}, \boldsymbol{v}) &:= \int_\Omega \boldsymbol{u}\cdot\boldsymbol{v}\, dx, \quad c(p, q) := \int_\Omega \frac{1}{\lambda(x)} p\, q\, dx, \end{aligned}$$

for all $\boldsymbol{u}, \boldsymbol{v} \in \mathrm{H}$, and $p, q \in \mathrm{Q}$.

To perform the analysis, we need a suitable norm which in particular depends on the parameters of the problem. With this in mind, and for all $(\boldsymbol{v}, q) \in \mathrm{H} \times Q$, we define the following weighted norm,

$$|||(\boldsymbol{v}, q)|||^2_{\mathrm{H}\times Q} := \|\mu(x)^{1/2}\nabla\boldsymbol{v}\|^2_{0,\Omega} + \|\mu(x)^{-1/2}q\|^2_{0,\Omega} + \|\lambda(x)^{-1/2}q\|^2_{0,\Omega}.$$

Moreover, in what follows, we assume that $\mu(x), 1/\lambda(x) \in \mathrm{W}^{1,\infty}(\Omega)$.

Let us introduce and define the kernel of $b(\cdot,\cdot)$ by

$$\mathrm{X} := \{\boldsymbol{v} \in \mathrm{H} \,:\, b(\boldsymbol{v}, q) = 0, \quad \forall\, q \in Q\} \,=\, \{\boldsymbol{v} \in \mathrm{H} \,:\, \operatorname{div}\boldsymbol{v} \,=\, 0 \ \text{ in } \Omega\},$$

and let us recall that the bilinear form $b(\cdot,\cdot)$ satisfies the inf-sup condition:

$$\sup_{\substack{\boldsymbol{v}\in \mathrm{H}\\ \boldsymbol{v}\neq 0}} \frac{|b(\boldsymbol{v},q)|}{\|\mu(x)^{1/2}\nabla \boldsymbol{v}\|_{0,\Omega}} \geq \beta_2 \|\mu(x)^{-1/2} q\|_{0,\Omega} \quad \forall q \in \mathrm{Q}, \tag{2.6}$$

with an inf-sup constant $\beta_2 > 0$ only depending on $\Omega$; see [14], for instance.

Now, we are in a position to introduce the solution operator which we denote by $\boldsymbol{T}_\nu : \mathrm{L}^2(\Omega)^d \to \mathrm{L}^2(\Omega)^d$ and is such that $\boldsymbol{f} \mapsto \boldsymbol{T}_\nu \boldsymbol{f} := \widehat{\boldsymbol{u}}$, where the pair $(\widehat{\boldsymbol{u}}, \widehat{p}) \in \mathrm{H}\times\mathrm{Q}$ is the solution of the following well posed source problem: Given $\boldsymbol{f} \in \mathrm{L}^2(\Omega)^d$ find $(\widehat{\boldsymbol{u}}, \widehat{p}) \in \mathrm{H}\times\mathrm{Q}$ such that

$$\begin{cases} a(\widehat{\boldsymbol{u}}, \boldsymbol{v}) + b(\boldsymbol{v}, \widehat{p}) = d(\boldsymbol{f}, \boldsymbol{v}) \ \forall \boldsymbol{v} \in \mathrm{H}, \\ b(\widehat{\boldsymbol{u}}, q) - c(\widehat{p}, q) = 0 \qquad \forall q \in \mathrm{Q}. \end{cases} \tag{2.7}$$

Thanks to the Babuška-Brezzi theory we have that $\boldsymbol{T}_\nu$ is well defined and the following estimate holds

$$\|\boldsymbol{T}_\nu \boldsymbol{f}\|_{0,\Omega} \leq |||(\boldsymbol{T}_\nu \boldsymbol{f}, \widehat{p})||| \lesssim \|\boldsymbol{f}\|_{0,\Omega},$$

with a constant depending on the inverse of $\mu$ and the Poincaré constant. It is easy to check that $\boldsymbol{T}_\nu$ is a selfadjoint operator with respect to the $\mathrm{L}^2$ inner product. Also, let $\chi$ be a real number such that $\chi \neq 0$. Notice that $(\chi, \boldsymbol{u}) \in \mathbb{R}\times\mathrm{H}$ is an eigenpair of $\boldsymbol{T}_\nu$ if and only if there exists $p \in \mathrm{Q}$ such that, $(\kappa, (\boldsymbol{u}, p))$ solves problem (2.5) with $\chi := 1/\kappa$.

The following result states an additional regularity result for problem (2.7).

**Lemma 2.1** *Let $(\widehat{\boldsymbol{u}}, \widehat{p})$ be the unique solution of (2.7), then there exists $s \in (0,1]$ such that $(\widehat{\boldsymbol{u}}, \widehat{p}) \in \mathrm{H}^{1+s}(\Omega)^d \times \mathrm{H}^s(\Omega)$ and the following estimate holds (see for instance [12] or [17])*

$$\|\widehat{\boldsymbol{u}}\|_{1+s,\Omega} + \|\widehat{p}\|_{s,\Omega} \lesssim \|\boldsymbol{f}\|_{0,\Omega},$$

*where the hidden constant depends on $\Omega$ and the Lamé coefficients.*

Let us remark that Lemma 2.1 holds true even for $\lambda \uparrow \infty$ (Further comments on this fact can be seen in [16]).

As a consequence of this result, we conclude compactness of $\boldsymbol{T}_\nu$. In fact, since $\mathrm{H}^{1+s}(\Omega)^d \hookrightarrow \mathrm{L}^2(\Omega)^d$ we have that $\boldsymbol{T}_\nu$ is a compact operator. Hence, we are in position to establish the spectral characterization of $\boldsymbol{T}_\nu$.

**Theorem 2.1** *The spectrum of $\boldsymbol{T}_\nu$ satisfies $\mathrm{sp}(\boldsymbol{T}_\nu) = \{0\} \cup \{\chi_k\}_{k\in\mathbb{N}}$, where $\{\chi_k\}_{k\in\mathbb{N}}$ is a sequence of positive eigenvalues.*

On the other hand, from [10] we have the following regularity result for the eigenfunctions of the eigenproblem (2.5).

**Theorem 2.2** *If $(\kappa, (\boldsymbol{u}, p)) \in \mathbb{R}\times\mathrm{H}\times\mathrm{Q}$ solves (2.5), then, there exists $r > 0$ such that $\boldsymbol{u} \in \mathrm{H}^{1+r}(\Omega)^d$ and $p \in \mathrm{H}^r(\Omega)$. Moreover, the following estimate holds*

$$\|\boldsymbol{u}\|_{1+r,\Omega} + \|p\|_{r,\Omega} \lesssim \|\boldsymbol{u}\|_{0,\Omega}.$$

Now, Let us end this section introducing the bilinear form $\mathcal{A} : (\mathrm{H}\times\mathrm{Q}) \times (\mathrm{H}\times\mathrm{Q}) \to \mathbb{R}$ defined by

$$\mathcal{A}((\boldsymbol{u}, p), (\boldsymbol{v}, q)) := a(\boldsymbol{u}, \boldsymbol{v}) + b(\boldsymbol{v}, p) + b(\boldsymbol{u}, q) + c(p, q), \tag{2.8}$$

which allows us to rewrite the eigenvalue problem as follows. Find $\kappa \in \mathbb{R}$ and $(\boldsymbol{0}, 0) \neq (\boldsymbol{u}, p) \in \mathrm{H}\times\mathrm{Q}$ such that

$$\mathcal{A}((\boldsymbol{u}, p), (\boldsymbol{v}, q)) = \kappa d(\boldsymbol{u}, \boldsymbol{v}) \quad \forall (\boldsymbol{v}, q) \in \mathrm{H}\times Q.$$

Let us remark that $\mathcal{A}(\cdot,\cdot)$ is a bounded bilinear form, in the sense that there exists a positive constant $\widehat{C} := \max\{2, \mu_{min}^{-1/2}\mu_{max}^{1/2}\}$ such that

$$\mathcal{A}((\boldsymbol{u}, p), (\boldsymbol{v}, q)) \leq \widehat{C} |||(\boldsymbol{u}, p)|||_{\mathrm{H}\times Q} |||(\boldsymbol{v}, q)|||_{\mathrm{H}\times Q} \quad \forall (\boldsymbol{u}, p), (\boldsymbol{v}, q) \in \mathrm{H}\times\mathrm{Q}.$$

Next we state the stability result for the bilinear form $\mathcal{A}$.

**Lemma 2.2** *For any* $(\boldsymbol{u}, p) \in \mathrm{H} \times \mathrm{Q}$*, there exists* $(\boldsymbol{v}, q) \in \mathrm{H} \times \mathrm{Q}$ *with* $|||(\boldsymbol{v}, q)||| \lesssim |||(\boldsymbol{u}, p)|||$ *such that*

$$|||(\boldsymbol{u}, p)|||^2 \lesssim \mathcal{A}((\boldsymbol{u}, p), (\boldsymbol{v}, q)).$$

*Proof* Recalling the definition of the bilinear form $\mathcal{A}(\cdot, \cdot)$, we find

$$\mathcal{A}((\boldsymbol{u}, p), (\boldsymbol{u}, -p)) = \|(2\mu)^{1/2}\boldsymbol{\varepsilon}(\boldsymbol{u})\|_{0,\Omega}^2 + \|\lambda^{-1/2}p\|_{0,\Omega}^2.$$

Thanks to inf-sup condition (2.6), for any $p \in \mathrm{Q}$, we find $\tilde{\boldsymbol{v}} \in \mathrm{H}$ with $\|(2\mu)^{1/2}\boldsymbol{\varepsilon}(\tilde{\boldsymbol{v}})\|_{0,\Omega} \leq C_1\|(2\mu)^{-1/2}p\|_{0,\Omega}$ such that $C_2\|(2\mu)^{-1/2}p\|_{0,\Omega}^2 \leq b(\tilde{\boldsymbol{v}}, p)$. This allows us to conclude that

$$\begin{aligned}\mathcal{A}((\boldsymbol{u}, p), (\tilde{\boldsymbol{v}}, 0)) = a(\boldsymbol{u}, \tilde{\boldsymbol{v}}) + b(\tilde{\boldsymbol{v}}, p) &\geq C_2\|(2\mu)^{-1/2}p\|_{0,\Omega}^2 - C_1\|(2\mu)^{1/2}\boldsymbol{\varepsilon}(\boldsymbol{u})\|_{0,\Omega}\|(2\mu)^{-1/2}p||_{0,\Omega} \\ &\geq (C_2 - 1/2\epsilon)\|(2\mu)^{-1/2}p||_{0,\Omega}^2 - (C_1^2\epsilon/2)\|(2\mu)^{1/2}\boldsymbol{\varepsilon}(\boldsymbol{u})||_{0,\Omega}.\end{aligned}$$

Making the specific choices $\boldsymbol{v} := \boldsymbol{u} + \delta\tilde{\boldsymbol{v}}$ and $q = -p$, we have

$$\begin{aligned}\mathcal{A}((\boldsymbol{u}, p), (\boldsymbol{v}, q)) &= \mathcal{A}((\boldsymbol{u}, p), (\boldsymbol{u}, -p)) + \delta\mathcal{A}((\boldsymbol{u}, p), (\tilde{\boldsymbol{v}}, 0)) \\ &\geq \|(2\mu)^{1/2}\boldsymbol{\varepsilon}(\boldsymbol{u})\|_{0,\Omega}^2 + \|\lambda^{-1/2}p\|_{0,\Omega}^2 \\ &\quad + \delta((C_2 - 1/2\epsilon)\|(2\mu)^{-1/2}p\|_{0,\Omega}^2 - (C_1^2\epsilon/2)\|(2\mu)^{1/2}\boldsymbol{\varepsilon}(\boldsymbol{u})\|_{0,\Omega})\end{aligned}$$

Choosing $\epsilon = 1/C_2$ and $\delta = C_2/C_1^2$ gives $\mathcal{A}((\boldsymbol{u}, p), (\boldsymbol{v}, q)) \gtrsim |||(\boldsymbol{u}, p)|||^2$. Additionally, we have

$$|||(\boldsymbol{v}, q)|||^2 = |||(\boldsymbol{u} + \delta\tilde{\boldsymbol{v}}, -p)|||^2 \lesssim |||(\boldsymbol{u}, p)|||^2.$$

The proof is complete.

## 2.2 The limit problem

The solution operator $\boldsymbol{T}_\nu$ depends strongly on the values of the Poisson ratio. This must be understood in the sense that there exists a family of problems depending on $\nu$ that $\boldsymbol{T}_\nu$ must solve. As we observe on the definition of the bilinear form $c(\cdot, \cdot)$, when $\lambda$ blows up, i.e. $\lambda \uparrow \infty$, then $c(\cdot, \cdot) \downarrow 0$ and hence, we are in presence of a Stokes-type of problem. So the natural question is what happens with the spectrum of $\boldsymbol{T}_\nu$ when $\lambda \uparrow \infty$. Let us begin by introducing the following eigenvalue problem: Find $(\kappa_0, (\boldsymbol{u}_0, p_0)) \in \mathbb{R} \times \mathrm{H} \times \mathrm{Q}$ such that

$$\begin{cases} a(\boldsymbol{u}_0, \boldsymbol{v}) + b(\boldsymbol{v}, p_0) = \kappa_0 d(\boldsymbol{u}_0, \boldsymbol{v}) & \forall \boldsymbol{v} \in \mathrm{H}, \\ b(\boldsymbol{u}_0, q) = 0 & \forall q \in \mathrm{Q}. \end{cases} \tag{2.9}$$

For this eigenvalue problem, let us introduce the following solution operator $\boldsymbol{T}_0 : \mathrm{L}^2(\Omega)^d \to \mathrm{L}^2(\Omega)^d$ defined by $\boldsymbol{f} \mapsto \boldsymbol{T}_0\boldsymbol{f} := \widehat{\boldsymbol{u}}_0$, where the pair $(\widehat{\boldsymbol{u}}_0, \widehat{p}_0)$ solves the following source problem: Find $(\widehat{\boldsymbol{u}}_0, \widehat{p}_0) \in \mathrm{H} \times \mathrm{Q}$ such that

$$\begin{cases} a(\widehat{\boldsymbol{u}}_0, \boldsymbol{v}) + b(\boldsymbol{v}, \widehat{p}_0) = d(\boldsymbol{f}, \boldsymbol{v}) & \forall \boldsymbol{v} \in \mathrm{H}, \\ b(\widehat{\boldsymbol{u}}_0, q) = 0 & \forall q \in \mathrm{Q}. \end{cases} \tag{2.10}$$

This operator $\boldsymbol{T}_0$ is well defined, self-adjoint, and compact and its spectral characterization is given as follows.

**Lemma 2.3** *The spectrum of* $\boldsymbol{T}_0$ *satisfies* $\mathrm{sp}(\boldsymbol{T}_0) = \{0\} \cup \{\chi_k^0\}_{k\in\mathbb{N}}$*, where* $\{\chi_k^0\}_{k\in\mathbb{N}}$ *is a sequence of positive eigenvalues such that* $\chi_k^0 \downarrow 0$ *as* $k \uparrow +\infty$*.*

For the operators $\boldsymbol{T}_\nu$ and $\boldsymbol{T}_0$, we have the following result.

**Lemma 2.4** *The following estimate holds*

$$\|(\boldsymbol{T}_\nu - \boldsymbol{T}_0)\boldsymbol{f}\|_{0,\Omega} \leq |||(\boldsymbol{T}_\nu - \boldsymbol{T}_0)\boldsymbol{f}||| \lesssim \|\lambda^{-1/2}\widehat{p}_0\|_{0,\Omega} \lesssim (2(1-2\nu)/\nu)^{1/2}\|\boldsymbol{f}\|_{0,\Omega}, \quad \forall \boldsymbol{f} \in \mathrm{L}^2(\Omega)^d, \tag{2.11}$$

*where the hidden constants are independent of the Poisson ratio.*

*Proof* Let $\boldsymbol{f} \in \mathrm{L}^2(\Omega)^d$. Subtracting (2.10) from (2.7) we obtain

$$\begin{aligned} 2\int_\Omega \mu(x)\boldsymbol{\varepsilon}(\widehat{\boldsymbol{u}} - \widehat{\boldsymbol{u}}_0) : \boldsymbol{\varepsilon}(\boldsymbol{v})\,dx - \int_\Omega (\widehat{p} - \widehat{p}_0)\operatorname{div}\boldsymbol{v}\,dx = 0 \quad \forall \boldsymbol{v} \in \mathrm{H} \\ -\int_\Omega q\operatorname{div}(\widehat{\boldsymbol{u}} - \widehat{\boldsymbol{u}}_0)\,dx + \int_\Omega \frac{\widehat{p}q}{\lambda}\,dx = 0 \quad \forall q \in \mathrm{Q}. \end{aligned}$$

Moreover, it also holds:

$$\begin{aligned} 2\int_\Omega \mu\boldsymbol{\varepsilon}(\widehat{\boldsymbol{u}} - \widehat{\boldsymbol{u}}_0) : \boldsymbol{\varepsilon}(\boldsymbol{v}) - \int_\Omega (\widehat{p} - \widehat{p}_0)\operatorname{div}\boldsymbol{v} = 0 \quad \forall \boldsymbol{v} \in \mathrm{H} \\ -\int_\Omega q\operatorname{div}(\widehat{\boldsymbol{u}} - \widehat{\boldsymbol{u}}_0) + \int_\Omega \frac{(\widehat{p} - \widehat{p}_0)q}{\lambda} = -\int_\Omega \frac{\widehat{p}_0 q}{\lambda} \quad \forall q \in \mathrm{Q}. \end{aligned}$$

Using stability result gives:

$$|||(\widehat{\boldsymbol{u}} - \widehat{\boldsymbol{u}}_0, \widehat{p} - \widehat{p}_0)||| \lesssim \|\lambda^{-1/2}\widehat{p}_0\|_{0,\Omega} \lesssim (2(1-2\nu)/\nu)^{1/2}\|\mu(x)^{-1/2}\boldsymbol{f}\|_{0,\Omega}.$$

This concludes the proof.

As a consequence of this result, $\boldsymbol{T}_\nu$ converges to $\boldsymbol{T}_0$ as $h \downarrow 0$. Then we have that standard properties of separation of isolated parts of the spectrum yield the following result:

**Lemma 2.5** *Let $\chi^0 > 0$ be an eigenvalue of $\boldsymbol{T}_0$ of multiplicity $m$. Let $D$ be any disc in the complex plane centered at $\chi^0$ and containing no other element of the spectrum of $\boldsymbol{T}_0$. Then, for $\nu$ goes to $\frac{1}{2}$, $D$ contains exactly $m$ eigenvalues of $\boldsymbol{T}_\nu$ (repeated according to their respective multiplicities). Consequently, each eigenvalue $\chi^0 > 0$ of $\boldsymbol{T}_0$ is a limit of eigenvalues $\chi > 0$ of $\boldsymbol{T}_\nu$, as $\nu$ goes to $\frac{1}{2}$.*

## 3 Numerical discretization

In this section our aim is to describe a finite element discretization of problem (2.5). To do this task, we will introduce two families of inf-sup stable finite elements whose properties also hold for the eigenvalue problem. We begin by introducing some preliminary definitions and notations to perform the analysis. Let $\mathcal{T}_h = \{T\}$ be a conforming partition of $\overline{\Omega}$ into closed simplices $T$ with size $h_T = \operatorname{diam}(T)$. Define $h := \max_{T\in\mathcal{T}_h} h_T$. Given a mesh $\mathcal{T}_h \in \mathbb{T}$, we denote by $\mathrm{H}_h$ and $\mathrm{Q}_h$ the finite element spaces that approximate the velocity field and the pressure, respectively. In particular, our study is focused in the following two elections:

(a) The mini element [9, Section 4.2.4]: Here,

$$\begin{aligned} \mathrm{H}_h &= \{\boldsymbol{v}_h \in \boldsymbol{C}(\overline{\Omega}) \ : \ \boldsymbol{v}_h|_T \in [\mathbb{P}_1(T) \oplus \mathbb{B}(T)]^d \ \forall\, T \in \mathcal{T}_h\} \cap \mathrm{H}, \\ \mathrm{Q}_h &= \{q_h \in C(\overline{\Omega}) \ : \ q_h|_T \in \mathbb{P}_1(T) \ \forall\, T \in \mathcal{T}_h\} \cap \mathrm{Q}, \end{aligned}$$

where $\mathbb{B}(T)$ denotes the space spanned by local bubble functions.

(b) The lowest order Taylor–Hood element [9, Section 4.2.5]: In this case,

$$\begin{aligned} \mathrm{H}_h &= \{\boldsymbol{v}_h \in \boldsymbol{C}(\overline{\Omega}) \ : \ \boldsymbol{v}_h|_T \in [\mathbb{P}_2(T)]^d \ \forall\, T \in \mathcal{T}_h\} \cap \mathrm{H}, \\ \mathrm{Q}_h &= \{q_h \in C(\overline{\Omega}) \ : \ q_h|_T \in \mathbb{P}_1(T) \ \forall\, T \in \mathcal{T}\} \cap \mathrm{Q}. \end{aligned}$$

The discrete analysis will be performed in a general manner, where the both families of finite elements, namely Taylor-Hood and mini element, are considered with no difference. If some difference must be claimed, we will point it out when is necessary.

### 3.1 The discrete eigenvalue problem

Now we are in position to introduce the discrete counterpart of the eigenvalue problem (2.5): Find $(\kappa_h, \boldsymbol{u}_h, p_h) \in \mathbb{R} \times \mathrm{H} \times \mathrm{Q}$ such that

$$\begin{cases} a(\boldsymbol{u}_h, \boldsymbol{v}_h) + b(\boldsymbol{v}_h, p_h) = \kappa_h d(\boldsymbol{u}_h, \boldsymbol{v}_h) \ \forall \boldsymbol{v}_h \in \mathrm{H}_h, \\ b(\boldsymbol{u}_h, q_h) - c(p_h, q_h) = 0 \qquad\qquad\quad \forall q_h \in \mathrm{Q}_h. \end{cases} \tag{3.1}$$

Since the choice of mini element and Taylor-Hood are inf-sup stable, we are in position to introduce the discrete solution operator $\boldsymbol{T}_{\nu,h} : \mathrm{L}^2(\Omega)^d \to \mathrm{H}_h$ defined by $\boldsymbol{f} \mapsto \boldsymbol{T}_{\nu,h} := \widehat{\boldsymbol{u}}_h$, where the pairs $(\widehat{\boldsymbol{u}}_h, \widehat{p}_h) \in \mathrm{H}_h \times \mathrm{Q}_h$ solves the following discrete source problem

$$\begin{cases} a(\widehat{\boldsymbol{u}}_h, \boldsymbol{v}_h) + b(\boldsymbol{v}_h, \widehat{p}_h) = d(\boldsymbol{f}, \boldsymbol{v}_h) \ \forall \boldsymbol{v}_h \in \mathrm{H}_h, \\ b(\widehat{\boldsymbol{u}}_h, q_h) - c(\widehat{p}_h, q_h) = 0 \qquad\quad \forall q_h \in \mathrm{Q}_h. \end{cases}$$

This problem is clearly well posed and the solutions satisfies the following estimate

$$\|\widehat{\boldsymbol{u}}_h\|_{0,\Omega} \leq |||(\widehat{\boldsymbol{u}}_h, \widehat{p}_h)||| \lesssim \|\boldsymbol{f}\|_{0,\Omega}.$$

As in the continuous case, we have that $\kappa_h$ is an eigenvalue of problem (3.1) if and only if $\chi_h := \dfrac{1}{\kappa_h}$ is an eigenvalue of $\boldsymbol{T}_{\nu,h}$ with the same multiplicity and corresponding eigenfunctions.

Moreover, if $\mathcal{L}_h$ represents the Lagrange interpolator operator and $\mathcal{P}_h$ represents the $\mathrm{L}^2$-projection, the solutions of the continuous and discrete problems satisfy

$$\begin{aligned} |||(\widehat{\boldsymbol{u}} - \widehat{\boldsymbol{u}}_h, \widehat{p} - \widehat{p}_h)|||^2 &\lesssim \inf_{(\boldsymbol{v},q)\in \mathrm{H}_h\times\mathrm{Q}_h} |||(\widehat{\boldsymbol{u}} - \boldsymbol{v}, \widehat{p} - q)|||^2 \lesssim |||(\widehat{\boldsymbol{u}} - \mathcal{L}_h\widehat{\boldsymbol{u}}, \widehat{p} - \mathcal{P}_h\widehat{p})|||^2 \\ &= \left(\|\mu(x)^{1/2}\nabla(\widehat{\boldsymbol{u}} - \mathcal{L}_h\widehat{\boldsymbol{u}})\|^2_{0,\Omega} + \|\mu(x)^{-1/2}(\widehat{p} - \mathcal{P}_h\widehat{p})\|^2_{0,\Omega} + \|\lambda(x)^{-1/2}(\widehat{p} - \mathcal{P}_h\widehat{p})\|^2_{0,\Omega}\right) \\ &\lesssim \left(E_{\max}\|\nabla(\widehat{\boldsymbol{u}} - \mathcal{L}_h\widehat{\boldsymbol{u}})\|^2_{0,\Omega} + E_{\min}^{-1}\|(\widehat{p} - \mathcal{P}_h\widehat{p})\|_{0,\Omega} + E_{\min}^{-1}(1-2\nu)\|(\widehat{p} - \mathcal{P}_h\widehat{p})\|_{0,\Omega}\right) \\ &\lesssim h^{2s}\max\{E_{\max}, E_{\min}^{-1}(1+(1-2\nu))\}\left(\|\widehat{\boldsymbol{u}}\|^2_{1+s,\Omega} + \|\widehat{p}\|^2_{s,\Omega}\right), \end{aligned}$$

Hence, from Lemma 2.1 we obtain

$$|||(\widehat{\boldsymbol{u}} - \widehat{\boldsymbol{u}}_h, \widehat{p} - \widehat{p}_h)||| \lesssim h^s\left(\|\widehat{\boldsymbol{u}}\|_{1+s,\Omega} + \|\widehat{p}\|_{s,\Omega}\right) \lesssim h^s\|\boldsymbol{f}\|_{0,\Omega}. \tag{3.2}$$

Similar as the continuous case, with the aid of the bilinear form $\mathcal{A}(\cdot,\cdot)$ (cf. (2.8)) we can rewrite the discrete eigenvalue problem (3.1) as follows: Find $\kappa_h \in \mathbb{R}$ and $(\boldsymbol{0}, 0) \neq (\boldsymbol{u}_h, p_h) \in \mathrm{H}_h \times \mathrm{Q}_h$ such that

$$\mathcal{A}((\boldsymbol{u}_h, p_h), (\boldsymbol{v}_h, q_h)) = \kappa_h d(\boldsymbol{u}_h, \boldsymbol{v}_h) \quad \forall (\boldsymbol{v}_h, q_h) \in \mathrm{H}_h \times \mathrm{Q}_h.$$

Now we prove an error estimate in $\mathrm{L}^2$ for the displacement which we prove by using a standard duality argument. This estimate will be helpful to establish the convergence in norm of the solution operators.

**Lemma 3.1** *There following estimate holds*

$$||\widehat{\boldsymbol{u}} - \widehat{\boldsymbol{u}}_h||_{0,\Omega} \lesssim h^s|||(\widehat{\boldsymbol{u}} - \widehat{\boldsymbol{u}}_h, \widehat{p} - \widehat{p}_h)|||.$$

*where the hidden constant is independent of $\nu$ and $s$ is as in Lemma 2.1.*

*Proof* Assume that $(\widehat{\phi}, \widehat{\psi}) \in \mathrm{H} \times \mathrm{Q}$ solves the following dual source problem

$$\mathcal{A}((\widehat{\phi}, \widehat{\psi}), (\boldsymbol{v}, q)) = d(\widehat{\boldsymbol{u}} - \widehat{\boldsymbol{u}}_h, \boldsymbol{v}) \qquad \forall (\boldsymbol{v}, q) \in \mathrm{H} \times \mathrm{Q},$$

Let us assume that $(\widehat{\phi},\widehat{\psi})$ is the unique solution of (2.7), then there exists $s\in(0,1]$ such that the following estimate holds

$$\|\widehat{\phi}\|_{1+s,\Omega}+\|\widehat{\psi}\|_{s,\Omega}\lesssim\|\widehat{\boldsymbol{u}}-\widehat{\boldsymbol{u}}_h\|_{0,\Omega}. \tag{3.3}$$

Making a specific choice $\boldsymbol{v}=\widehat{\boldsymbol{u}}-\widehat{\boldsymbol{u}}_h$ and $q=\widehat{p}-\widehat{p}_h$, we find that

$$||\widehat{\boldsymbol{u}}-\widehat{\boldsymbol{u}}_h||_{0,\Omega}^2=\mathcal{A}((\widehat{\phi},\widehat{\psi}),(\widehat{\boldsymbol{u}}-\widehat{\boldsymbol{u}}_h,\widehat{p}-\widehat{p}_h)).$$

Using the fact that $\mathcal{A}((\widehat{\boldsymbol{u}}-\widehat{\boldsymbol{u}}_h,\widehat{p}-\widehat{p}_h),(\widehat{\phi}_h,\widehat{\psi}_h))=0$ we obtain

$$||\widehat{\boldsymbol{u}}-\widehat{\boldsymbol{u}}_h||_{0,\Omega}^2=\mathcal{A}((\widehat{\phi}-\widehat{\phi}_h,\widehat{\psi}-\widehat{\psi}_h),(\widehat{\boldsymbol{u}}-\widehat{\boldsymbol{u}}_h,\widehat{p}-\widehat{p}_h)).$$

Using the Cauchy-Schwarz, estimate (3.3), the approximation results and the stability result leads to the stated result.

Let us prove the key result that establish the convergence of $\boldsymbol{T}_{\nu,h}$ to $\boldsymbol{T}_\nu$ as $h\downarrow 0$.

**Lemma 3.2** *Given $\boldsymbol{f}\in\mathrm{L}^2(\Omega)^d$, the following estimate holds, independent of $\nu$, such that*

$$\|(\boldsymbol{T}_\nu-\boldsymbol{T}_{\nu,h})\boldsymbol{f}\|_{0,\Omega}\lesssim h^{2s}\|\boldsymbol{f}\|_{0,\Omega},$$

*where the hidden constant is independent of $\nu$ and $s$ is as in Lemma 2.1.*

*Proof* Let $\boldsymbol{f}\in\mathrm{L}^2(\Omega)^d$. Then

$$\|(\boldsymbol{T}_\nu-\boldsymbol{T}_{\nu,h})\boldsymbol{f}\|_{1,\Omega}=\|\widehat{\boldsymbol{u}}-\widehat{\boldsymbol{u}}_h\|_{1,\Omega}=\|\widehat{\boldsymbol{u}}-\widehat{\boldsymbol{u}}_h\|_{0,\Omega}+\|\nabla(\widehat{\boldsymbol{u}}-\widehat{\boldsymbol{u}}_h)\|_{0,\Omega}.$$

For the gradient error we have

$$\begin{aligned}\|\nabla(\widehat{\boldsymbol{u}}-\widehat{\boldsymbol{u}}_h)\|_{0,\Omega}&\lesssim\mu_{\min}^{-1/2}\|\mu(x)^{1/2}\nabla(\widehat{\boldsymbol{u}}-\widehat{\boldsymbol{u}}_h)\|_{0,\Omega}\\&\lesssim\mu_{\min}^{-1/2}\|\mu(x)^{1/2}\nabla(\widehat{\boldsymbol{u}}-\widehat{\boldsymbol{u}}_h)\|_{0,\Omega}+\|\mu(x)^{-1/2}(\widehat{p}-\widehat{p}_h)\|_{0,\Omega}+\|\lambda(x)^{-1/2}(\widehat{p}-\widehat{p}_h)\|_{0,\Omega}\\&\lesssim h^s\max\{\mu_{\min}^{-1/2},1\}\,(\|\widehat{\boldsymbol{u}}\|_{1+s,\Omega}+\|\widehat{p}\|_{s,\Omega})\lesssim h^s\max\{\mu_{\min}^{-1/2},1\}\|\boldsymbol{f}\|_{0,\Omega},\end{aligned} \tag{3.4}$$

where we have used the definition of $|||\cdot|||$ and (3.2). On the other hand, the error $\|\widehat{\boldsymbol{u}}-\widehat{\boldsymbol{u}}_h\|_{0,\Omega}$ is clearly estimated, first by Lemma 3.1 and then by (3.2) leading to

$$\|\widehat{\boldsymbol{u}}-\widehat{\boldsymbol{u}}_h\|_{0,\Omega}\lesssim h^{2s}\|\boldsymbol{f}\|_{0,\Omega}. \tag{3.5}$$

Finally, combining (3.5) and (3.4) we conclude the proof.

From the previous lemma, we can conclude the convergence in norm for $\boldsymbol{T}_{\nu,h}$ to $\boldsymbol{T}_\nu$ as $h\downarrow 0$. This is a key ingredient in order to obtain error estimates for eigenvalues and eigenfunctions. In fact, an immediate consequence of Lemma 3.2 is that isolated parts of $\mathrm{sp}(\boldsymbol{T}_\nu)$ are approximated by isolated parts of $\mathrm{sp}(\boldsymbol{T}_{\nu,h})$. It means that if $\chi$ is a nonzero eigenvalue of $\boldsymbol{T}_\nu$ with algebraic multiplicity $m$, hence there exist $m$ eigenvalues $\chi_h^{(1)},\ldots,\chi_h^{(m)}$ of $\boldsymbol{T}_{\nu,h}$ (repeated according to their respective multiplicities) that will converge to $\mu$ as $h$ goes to zero.

In what follows, we denote by $\mathfrak{E}$ the eigenspace of $\boldsymbol{T}_\nu$ associated to the eigenvalue $\chi$ and by $\mathfrak{E}_h$ the invariant subspace of $\boldsymbol{T}_{\nu,h}$ spanned by the eigenspaces of $\boldsymbol{T}_{\nu,h}$ associated to $\chi_h^{(1)},\ldots,\chi_h^{(m)}$.

Now our goal of this section is deriving error estimates for the eigenfunctions and eigenvalues. With this goal in mind, first we need to recall the definition of the gap $\widehat{\delta}$ between two closed subspaces $\mathcal{X}$ and $\mathcal{Y}$ of $\mathrm{L}^2(\Omega)$:

$$\widehat{\delta}(\mathcal{X},\mathcal{Y}):=\max\{\delta(\mathcal{X},\mathcal{Y}),\delta(\mathcal{X},\mathcal{Y})\},$$

where

$$\delta(\mathcal{X},\mathcal{Y}):=\sup_{x\in\mathcal{X}:\|x\|_{0,\Omega}=1}\left\{\inf_{y\in\mathcal{Y}}\quad\|x-y\|_{0,\Omega}\right\}.$$

We also define

$$\gamma_h := \sup_{\boldsymbol{v}\in\mathcal{E}:\|\boldsymbol{v}\|_{0,\Omega}=1} \|(\boldsymbol{T}_\nu - \boldsymbol{T}_{\nu,h})\boldsymbol{v}\|_{0,\Omega}.$$

In order to obtain $\nu$-independent error estimates, in what follows, we assume that $\chi$ is an eigenvalue of $\boldsymbol{T}_\nu$ converging to a simple eigenvalue $\chi_0$ of $\boldsymbol{T}_0$, as $\nu$ goes to $\frac{1}{2}$. The following error estimates for the approximation of eigenvalues and eigenfunctions hold true. The result can be obtained from from [4, Theorems 7.1 and 7.3].

**Theorem 3.1** *There exists a strictly positive constant $C$, independent of $\nu$ and $h$, such that*

$$\widehat{\delta}(\mathfrak{E}, \mathfrak{E}_h) \lesssim \gamma_h, \tag{3.6}$$

$$|\chi - \chi_h| \lesssim \gamma_h. \tag{3.7}$$

*Proof* On the one hand, We have that (3.6) is a direct consequence of Theorem 7.1 in [4], with a constant $C > 0$ depending on the constant in (3.5) (which is independent of $\nu$) and on the inverse of the distance of $\chi$ to the rest of the spectrum of $\boldsymbol{T}_\nu$. Then, from Lemma 2.5, (2.11) implies that for $\nu$ goes to $\frac{1}{2}$ this distance can be bounded below in terms of the distance of $\chi_0$ to the rest of the spectrum of $\boldsymbol{T}_0$, which does not depend on Poisson ratio. On the other hand, estimate (3.7) follows from Theorem 7.3 in [4].

Moreover, by using the additional regularity of the eigenfunctions, we obtain the following result.

**Theorem 3.2** *There following estimates hold*

$$\|(\boldsymbol{T}_\nu - \boldsymbol{T}_{\nu,h})\boldsymbol{v}\|_{0,\Omega} \lesssim h^{2r}\|\boldsymbol{v}\|_{0,\Omega} \qquad \forall \boldsymbol{v} \in \mathfrak{E}, \tag{3.8}$$

*and as a consequence,*

$$\gamma_h \lesssim h^{2r}, \tag{3.9}$$

*where the hidden constants are independent of $\nu$ and $h$ and $r > 0$ is as in Theorem 2.2.*

*Proof* The inequality (3.8) is obtained repeating the proof of Lemma 3.2 and Theorem 2.2. Estimate (3.9) follows from the definition of $\gamma_h$.

Finally, we have the following result for vibration frequencies of the elasticity eigenproblem, which is an immediate consequence of (3.7).

**Corollary 3.1** *The following estimate holds*

$$|\kappa - \kappa_h| \lesssim h^{2r},$$

*where the hidden constant is independent of $\nu$ and $h$ and $r > 0$ is as in Theorem 2.2.*

## 4 A posteriori error analysis

The aim of this section is to introduce a suitable residual-based error estimator for the Stokes/elasticity eigenvalue problem. The main aim is to prove that the proposed estimator is equivalent with the error. Moreover, on the forthcoming analysis we will focus only on eigenvalues with multiplicity 1. With this purpose, we introduce the following definitions and notations. For any element $K \in \mathcal{T}_h$, we denote by $\mathcal{E}_K$ the set of facets of $K$ and

$$\mathcal{E}_h := \bigcup_{K\in\mathcal{T}_h} \mathcal{E}_K.$$

We decompose $\mathcal{E}_h = \mathcal{E}_\Omega \cup \mathcal{E}_{\partial\Omega}$, where $\mathcal{E}_{\partial\Omega} := \{\ell \in \mathcal{E}_h : \ell \subset \partial\Omega\}$ and $\mathcal{E}_\Omega := \mathcal{E}\backslash\mathcal{E}_{\partial\Omega}$. For each inner edge $\ell \in \mathcal{E}_\Omega$ and for any sufficiently smooth function $\boldsymbol{v}$, we define the jump of its normal derivative on $\ell$ by

$$\left[\!\left[\frac{\partial \boldsymbol{v}}{\partial \boldsymbol{n}}\right]\!\right]_\ell := \nabla(\boldsymbol{v}|_K)\cdot \boldsymbol{n}_K + \nabla(\boldsymbol{v}|_{K'})\cdot \boldsymbol{n}_{K'},$$

where $K$ and $K'$ are the two elements in $\mathcal{T}_h$ sharing the edge $\ell$ and $\boldsymbol{n}_K$ and $\boldsymbol{n}_{K'}$ are the respective outer unit normal vectors.

### 4.1 Residual based a posteriori error estimator

The local element residual ($\eta_K$) and the edge jump-residual estimator ($\eta_J$) are defined as follows:

$$\eta_K^2 := h_K^2\|\rho_1 \mathbf{R}_{1,T}\|_{0,T}^2 + \|\rho_2^{1/2} R_{2,T}\|_{0,T}^2, \quad \eta_J^2 := h_E\|\rho_E J_\ell\|_{0,\ell}^2$$

where

$$\mathbf{R}_{1,T} := \mathbf{div}(2\mu_h \boldsymbol{\varepsilon}(\boldsymbol{u}_h)) - \nabla p_h + \rho\kappa \boldsymbol{u}_h \quad \text{and} \quad R_{2,T} := \operatorname{div} \boldsymbol{u}_h + \frac{1}{\lambda} p_h.$$

For the jump terms, we define

$$J_\ell := \begin{cases} \dfrac{1}{2}[\![(2\mu_h \boldsymbol{\varepsilon}(\boldsymbol{u}_h) - p_h \mathbb{I})\mathbf{n}]\!], & E \in \Omega \cap \mathcal{E}_h \\ (2\mu_h \boldsymbol{\varepsilon}(\boldsymbol{u}_h) - p_h \mathbb{I})\mathbf{n}, & E \in \Gamma_N \cap \mathcal{E}_h \\ \mathbf{0}, & E \in \Gamma_D \cap \mathcal{E}_h. \end{cases}$$

Here, the parameters $\rho_1$, $\rho_2$ and $\rho_3$ are defined by

$$\rho_{1,K} := (2\mu_h)^{-1/2}, \quad \rho_2 := \left[(2\mu_h)^{-1} + \lambda^{-1}\right]^{-1}, \quad \rho_E := (2\mu_h)^{-1/2}/\sqrt{2},$$

where $\mu_h$ correspond to the $\mathrm{L}^2$ polynomial projection of $\mu$. The local data oscillation is defined as $\Theta_K^2 = \|\rho_1(\mu - \mu_h)\boldsymbol{\varepsilon}(\boldsymbol{u}_h)\|_0^2$. Finally, we discuss the definition of the global a posteriori estimatior $\eta$ and the global data oscillation error as

$$\eta := \left(\sum_{K\in\mathcal{T}_h} \eta_K^2\right)^{1/2}, \quad \Theta := \left(\sum_{K\in\mathcal{T}_h} \Theta_K^2\right)^{1/2}.$$

### 4.2 Reliability

The task here is to prove that the error is upper bounded by the estimator, together with the high order terms. This is stated in the following result.

**Theorem 4.1 (Reliability)**

*Let $(\kappa, (\boldsymbol{u}, p)) \in \mathbb{R} \times \mathrm{H} \times \mathrm{Q}$ be a solution of the spectral problem (2.5) and let $(\kappa_h, (\boldsymbol{u}_h, p_h)) \in \mathbb{R} \times \mathrm{H}_h \times \mathrm{Q}_h$ be the finite element approximation of $(\kappa, (\boldsymbol{u}, p))$ given as the solution of (3.1). Then, for every $h_0 \geq h$ there holds*

$$|||(\boldsymbol{u} - \boldsymbol{u}_h, p - p_h)||| \lesssim \eta + \Theta + |\kappa - \kappa_h| + \kappa\|\boldsymbol{u} - \boldsymbol{u}_h\|_{0,\Omega}.$$

*where the hidden constant is independent of the mesh size, $\nu$ and the discrete solutions. Additionally, the following reliability of the eigenvalue also holds:*

$$|\kappa - \kappa_h| \lesssim \eta^2 + \Theta^2.$$

*Proof* Given $(\boldsymbol{v}, q) \in \mathrm{H}_h \times \mathrm{Q}_h$, we subtract the continuous formulation (cf. (2.5)) and its discrete counterpart (cf. (3.1)) in order to obtain the error equation

$$\mathcal{A}((\mathsf{e}_{\boldsymbol{u}}, \mathsf{e}_p), (\boldsymbol{v}, q)) = (\kappa \boldsymbol{u} - \kappa_h \boldsymbol{u}_h, \boldsymbol{v})_{0,\Omega} \quad \forall (\boldsymbol{v}, q) \in \mathrm{H}_h \times \mathrm{Q}_h. \tag{4.1}$$

Thanks to Lemma 2.2, we have that for $(\boldsymbol{u}, p) \in \mathrm{H} \times \mathrm{Q}$, there exists $(\boldsymbol{w}, r) \in \mathrm{H} \times \mathrm{Q}$, with

$$|||(\boldsymbol{w}, r)||| \lesssim |||(\boldsymbol{u} - \boldsymbol{u}_h, p - \widehat{p}_h)|||,$$

such that

$$|||(\boldsymbol{u} - \boldsymbol{u}_h, p - \widehat{p}_h)|||^2 \lesssim \mathcal{A}((\mathsf{e}_{\boldsymbol{u}}, \mathsf{e}_p), (\boldsymbol{w}, r)). \tag{4.2}$$

Let us define $\boldsymbol{w}_I \in \mathrm{H}_h$ as the Clément interpolant (see [15, Chapter 2]) and $r_I \in \mathrm{Q}_h$ as the standard $\mathrm{L}^2$-projection of $r$. Then, from (4.1) and (4.2) we obtain

$$\begin{aligned}
|||(\boldsymbol{u} - \boldsymbol{u}_h, p - p_h)||| &\leq \kappa(\boldsymbol{u}, \boldsymbol{w})_{0,\Omega} - \mathcal{A}((\boldsymbol{u}_h, p_h); (\boldsymbol{w}, r)) \\
&= (\kappa \boldsymbol{u} - \kappa_h \boldsymbol{u}_h, \boldsymbol{w})_{0,\Omega} + \kappa_h(\boldsymbol{u}_h, \boldsymbol{w} - \boldsymbol{w}_I)_{0,\Omega} - \mathcal{A}((\boldsymbol{u}_h, p_h); (\boldsymbol{w} - \boldsymbol{w}_I, r - r_I)) \\
&= \underbrace{-\mathcal{A}((\boldsymbol{u}_h, p_h); (\boldsymbol{w} - \boldsymbol{w}_I, r - r_I)) + (\kappa_h \boldsymbol{u}_h, \boldsymbol{w} - \boldsymbol{w}_I)_{0,\Omega}}_{\Lambda_1} + \underbrace{(\kappa \boldsymbol{u} - \kappa_h \boldsymbol{u}_h, \boldsymbol{w})_{0,\Omega}}_{\Lambda_2}.
\end{aligned}$$

An application of integration by parts together with Cauchy–Schwarz and the approximation results of the Clément interpolant gives

$$|\Lambda_1| \lesssim \eta |||(\boldsymbol{w}, r)|||, \quad |\Lambda_2| \lesssim \|\mu_h^{1/2}(\kappa \boldsymbol{u} - \kappa_h \boldsymbol{u}_h)\|_{0,\Omega} |||(\boldsymbol{w}, r)|||.$$

This completes the proof. Using

$$(\kappa - \kappa_h) d(\boldsymbol{u}_h, \boldsymbol{u}_h) = \mathcal{A}((\boldsymbol{u} - \boldsymbol{u}_h, p - p_h); (\boldsymbol{u} - \boldsymbol{u}_h, p - p_h)) - \kappa d(\boldsymbol{u} - \boldsymbol{u}_h, \boldsymbol{u} - \boldsymbol{u}_h)$$

with the above result leads to the second stated result.

### 4.3 Efficiency

The analysis for the efficiency follows the classic arguments based on bubble functions. An interior bubble function $\psi_K \in \mathrm{H}_0^1(K)$ for a polytope $K$ can be constructed piecewise as the sum of the cubic bubble functions for each tetrahedron of the sub-triangulation $\mathcal{T}_h^K$ that attain the value 1 at the barycenter of the tetrahedron. On the other hand, a facet bubble function $\psi_\ell$ for $\ell \in \partial K$ is a piecewise quadratic function attaining the value 1 at the barycenter of $\ell$ and vanishing on the polytope $K \in \mathcal{T}_h$ that do not contain $\ell$ on its boundary.

The following results which establish standard estimates for bubble functions will be useful in what follows (see [1,23]).

**Lemma 4.1 (Interior bubble functions)** *For any $K \in \mathcal{T}_h$, let $\psi_K$ be the corresponding interior bubble function. Then, there holds*

$$\begin{aligned}
&\|q\|_{0,K}^2 \lesssim \int_K \psi_K q^2 \leq \|q\|_{0,K}^2 \qquad \forall q \in \mathbb{P}_k(K), \\
&\|q\|_{0,K} \lesssim \|\psi_K q\|_{0,K} + h_K \|\nabla(\psi_K q)\|_{0,K} \lesssim \|q\|_{0,K} \qquad \forall q \in \mathbb{P}_k(K),
\end{aligned}$$

*where the hidden constants are independent of $h_K$.*

**Lemma 4.2 (Facet bubble functions)** *For any $K \in \mathcal{T}_h$ and $\ell \in \mathcal{E}_K$, let $\psi_\ell$ be the corresponding facet bubble function. Then, there holds*

$$\|q\|_{0,\ell}^2 \lesssim \int_\ell \psi_\ell q^2 \leq \|q\|_{0,\ell}^2 \qquad \forall q \in \mathbb{P}_k(\ell).$$

*Moreover, for all $q \in \mathbb{P}_k(\ell)$, there exists an extension of $q \in \mathbb{P}_k(K)$ (again denoted by $q$) such that*

$$h_K^{-1/2}\|\psi_\ell q\|_{0,K} + h_K^{1/2}\|\nabla(\psi_\ell q)\|_{0,K} \lesssim \|q\|_{0,\ell},$$

*where the hidden constants are independent of $h_K$.*

Now, we are in a position to establish the efficiency $\eta$, which is stated in the following result.

**Lemma 4.3** *(Efficiency) The following estimate holds*

$$\eta \lesssim |||(\boldsymbol{u}-\boldsymbol{u}_h, p-p_h)||| + \Theta + h.o.t,$$

*here the hidden constant is independent of the meshsize, $\nu$, and the discrete solution.*

*Proof* Also, we define $\boldsymbol{v}_T := \psi_T h_T^2 \rho_1^2 \mathbf{R}_{1,T}$, where $\psi_T$ is the bubble that satisfies the properties of Lemma 4.1. Now we compute a bound for the term $h_T^2\|\rho_1\mathbf{R}_{1,T}\|_{0,T}$. To do this task, let us recall that the continuous problem satisfies $-\mathbf{div}(2\mu(x)\boldsymbol{\varepsilon}(\boldsymbol{u})) + \nabla p - \rho\kappa\boldsymbol{u} = \mathbf{0}$. Hence

$$\begin{aligned} h_T^2\|\rho_1\mathbf{R}_{1,T}\|_{0,T}^2 &\leq \int_T (\mathbf{div}(2\mu_h(x)\boldsymbol{\varepsilon}(\boldsymbol{u}_h)) - \nabla p_h + \rho\kappa_h\boldsymbol{u}_h)\cdot\boldsymbol{v}_T \\ &= \int_T (-\mathbf{div}(2\mu_h(x)\boldsymbol{\varepsilon}(\mathtt{e}_{\boldsymbol{u}})) + \nabla \mathtt{e}_p + \rho\kappa_h\boldsymbol{u}_h - \rho\kappa\boldsymbol{u} - \mathbf{div}(2\mathtt{e}_\mu(x)\boldsymbol{\varepsilon}(\boldsymbol{u})))\cdot\boldsymbol{v}_T \\ &= \underbrace{\int_T (-\mathbf{div}(2\mu_h(x)\boldsymbol{\varepsilon}(\mathtt{e}_{\boldsymbol{u}})) + \nabla \mathtt{e}_p - \mathbf{div}(2\mathtt{e}_\mu(x)\boldsymbol{\varepsilon}(\boldsymbol{u})))\cdot\boldsymbol{v}_T}_{\mathrm{T}_1} + \underbrace{\int_T (\rho\kappa_h\boldsymbol{u}_h - \rho\kappa\boldsymbol{u})\cdot\boldsymbol{v}_T}_{\mathrm{T}_2}. \end{aligned}$$

To establish the bound of $\mathrm{T}_1$, we apply integration by parts which gives

$$\begin{aligned} T_1 &= \int_T (-\mathbf{div}(2\mu_h(x)\boldsymbol{\varepsilon}(\mathtt{e}_{\boldsymbol{u}})) + \nabla \mathtt{e}_p - \mathbf{div}(2\mathtt{e}_\mu(x)\boldsymbol{\varepsilon}(\boldsymbol{u})))\cdot\boldsymbol{v}_T \\ &= \int_T ((2\mu_h(x)\boldsymbol{\varepsilon}(\mathtt{e}_{\boldsymbol{u}})) - \mathtt{e}_p I + \mathtt{e}_\mu(x)\boldsymbol{\varepsilon}(\boldsymbol{u}))\cdot\nabla\boldsymbol{v}_T \leq (|||(\boldsymbol{u}-\boldsymbol{u}_h, p-p_h)|||_T + \Theta_K)h_T\|\rho_1\mathbf{R}_{1,T}\|_{0,T}. \end{aligned}$$

For the term $\mathrm{T}_2$ is enough to follow the proof of [19, Theorem 3.2] in order to obtain

$$\mathrm{T}_2 \lesssim h_T^2(|\kappa-\kappa_h| + \kappa\|\mathtt{e}_{\boldsymbol{u}}\|_{0,T})\|\rho_1\mathbf{R}_{1,T}\|_{0,T}.$$

Recalling the definition of $R_{2,T}$ and the continuous problem satisfies $\operatorname{div}\boldsymbol{u} + 1/\lambda\, p = 0$, we find

$$\|\rho_2^{1/2}R_{2,T}\|_{0,T} = \|\rho_2^{1/2}(\operatorname{div}(\boldsymbol{u}-\boldsymbol{u}_h + 1/\lambda(p-p_h))\|_{0,T} \lesssim |||(\boldsymbol{u}-\boldsymbol{u}_h, p-p_h)|||_T.$$

Next, we define $\boldsymbol{v}_\ell := \psi_\ell h_E \rho_E^2 [\![(2\mu_h\boldsymbol{\varepsilon}(\boldsymbol{u}_h) - p_h\mathbb{I})\mathbf{n}]\!]$, where $\psi_\ell$ is the bubble that satisfies the properties of Lemma 4.2. Now we compute a bound for the term $h_E\|\rho_E J_\ell\|_{0,\ell}^2$. Then, we obtain

$$h_E\|\rho_E J_\ell\|_{0,\ell}^2 \lesssim ([\![(2\mu_h\boldsymbol{\varepsilon}(\boldsymbol{u}_h) - p_h\mathbb{I})\mathbf{n}]\!], \boldsymbol{v}_\ell)_\ell = ([\![(2\mu_h\boldsymbol{\varepsilon}(\boldsymbol{u}_h) - 2\mu\boldsymbol{\varepsilon}(\boldsymbol{u}) - (p_h-p)\mathbb{I})\mathbf{n}]\!], \boldsymbol{v}_\ell)_\ell \tag{4.3}$$

Using Integration by parts on $\omega_T$ gives

$$\begin{aligned} ([\![(2\mu_h\boldsymbol{\varepsilon}(\boldsymbol{u}_h) - 2\mu\boldsymbol{\varepsilon}(\boldsymbol{u}) - (p_h-p)\mathbb{I})\mathbf{n}]\!], \boldsymbol{v}_\ell)_\ell = \sum_{T\in\omega_T} \Big( &(2\mu\boldsymbol{\varepsilon}(\boldsymbol{u}) - 2\mu_h(x)\boldsymbol{\varepsilon}(\boldsymbol{u}), \boldsymbol{\varepsilon}(\boldsymbol{v}_\ell))_T + (\mathtt{e}_p, \operatorname{div}\boldsymbol{v}_\ell)_T \\ &+ (\mathbf{R}_{1,T}, \boldsymbol{v}_\ell)_T + (\rho\kappa_h\boldsymbol{u}_h - \rho\kappa\boldsymbol{u}, \boldsymbol{v}_\ell)_T\Big). \end{aligned}$$

Applying Cauchy-Schwarz with Lemma 4.2 and combining with (4.3) implies that

$$h_E\|\rho_E J_\ell\|_{0,\ell}^2 \lesssim (|||(\boldsymbol{u}-\boldsymbol{u}_h, p-p_h)|||_{\omega_T} + \Theta_{\omega_T} + h.o.t.)h_E^{1/2}\|\rho_E J_\ell\|_{0,\ell}.$$

Combining the above estimates leads to the the stated efficiency result.

## 5 Numerical results

This section is devoted to analyze the performance of the proposed finite element method through different experiments, considering different values of $\mu$ and $\lambda$. The aim is to compare the computationally the spectrums of the Stokes limit and elasticity eigenvalue problems. To do this task, we have implemented a FEniCS script [2] for the codes. The meshes have been constructed using the GMSH software [11].

The convergence rates of the eigenvalues have been obtained with a standard least square fitting and highly refined meshes. The Taylor-Hood and mini-element families can be used indistinctively as observed in the theory provided in Section 2. Taylor-Hood elements will be preferred for the 2D and 3D representations, whereas the adaptive test are performed with the mini-element family.

We also denote by $N$ the mesh refinement level, whereas `dof` denotes the number of degrees of freedom. We denote by $\kappa_{h_i}$ the i-th discrete eigenfrequency, and by $\widehat{\kappa}_{h_i} := \kappa_{h_i}/(1+\nu)$ the unscaled version of $\kappa_{h_i}$.

Hence, we denote the error on the $i$-th eigenvalue by $\texttt{err}(\widehat{\kappa}_i)$ with

$$\texttt{err}(\widehat{\kappa}_i) := |\widehat{\kappa}_{h_i} - \widehat{\kappa}_i|.$$

We remark that computing $\sqrt{\widehat{\kappa}_{h_i}}$ or $\sqrt{\widehat{\kappa}_i}$ gives the corresponding discrete and exact eigenfrequency.

With the aim of assessing the performance of our estimator, we consider domains with singularities in two and three dimensions in order to observe the improvement of the convergence rate. On each adaptive iteration, we use the blue-green marking strategy to refine each $T' \in \mathcal{T}_h$ whose indicator $\eta_{T'}$ satisfies

$$\eta_{T'} \geq 0.5 \max\{\eta_T \,:\, T \in \mathcal{T}_h\}.$$

The effectivity indexes with respect to $\zeta$ and the eigenvalue $\widehat{\kappa}_i$ are defined by

$$\texttt{eff}(\widehat{\kappa}_i) := \frac{\texttt{err}(\widehat{\kappa}_i)}{\eta^2}.$$

### 5.1 2D square with constant Lamé parameters

In this experiment we test our method on the unit square domain $\Omega := (0,1)^2$. We borrow the experiment from [22, Section 6.1] consisting of a square domain, clamped at the bottom and free on the rest of the boundary. The physical parameters for this case are given by

$$E = 1.44 \times 10^{11}\text{Pa}, \quad \rho = 7.7 \times 10^{3}\text{Kg/m}^3.$$

The following values of $\nu$, together with their respective Sobolev exponent are potrayed in Table 1 (see for instance [12]). Tables 2 and 3 present the first six lowest order computed eigenfrequencies

| $\nu$ | $\mu$ | $\lambda$ | $r$ |
|---|---|---|---|
| 0.35 | 7.2000e+10 | 1.6800e+11 | 0.6797 |
| 0.49 | 7.2000e+10 | 3.5280e+12 | 0.5999 |
| 0.49999 | 7.2000e+10 | 3.5999e+15 | 0.5947 |
| 0.5 | 7.2000e+10 | $\infty$ | 0.5649 |

**Table 1** Test 5.1. Different values of $\nu$, together with the corresponding computed values of $\mu$, $\lambda$ and the Sobolev exponent.

compared with those of [22]. Here, we observe that, in both tables, the convergence rate for the

third and fifth mode behaves like $\mathcal{O}(h^r)$, with $r \geq 2$, whereas the rest of the modes converge to the extrapolated values with $2r \geq 1.36$ for $\nu = 0.35$, and $2r \geq 1.2$ for the Stokes limit case $\nu \approx 0.5$.

We now pass to adaptive refinements. Note that the results provided in Tables 2 - 3 shows that the first eigenvalue rate of convergence is suboptimal since we have point singularites, related to the change of boundary conditions, in $(x, y) = (0, 0)$ and $(x, y) = (1, 0)$. We study the adaptive refinements for the first eigenvalue. Figure 1 depicts the different convergence behavior for each value of $\nu$. It is clear that the optimal rate of convergence is recovered, behaving like $\mathcal{O}(\texttt{dof}^{-1}) \simeq \mathcal{O}(h^2)$. To study the behavior of the estimator, we have computed the values of $\eta^2$ and $\texttt{eff}(\lambda_1)$ on Figure 2. Here, we observe that the estimator behaves like $\mathcal{O}(h^2)$, yielding to a roughly constant efficiency behavior, which oscillates between 0.16 and 0.19 for the selected values of $\nu$. We also present the adaptive meshes on Figure 3, where we observe that the refinements are concentrated near the two singular corners. Also, the amount of elements marked for $\nu = 0.35$ is significantly higher than those marked in the limit case. This is associated to the additional contribution on the volumetric and jump terms associated to $\lambda$.

**Table 2** Test 5.1. Lowest computed eigenvalues for the mini-element family and different values of $\nu$.

| $N = 20$ | $N = 30$ | $N = 40$ | $N = 50$ | Order | $\sqrt{\widehat{\kappa}_{extr}}$ | [22] |
|---|---|---|---|---|---|---|
| $\nu = 0.35$ | | | | | | |
| 2967.3574 | 2957.0361 | 2952.7091 | 2950.4117 | 1.53 | 2944.7395 | 2944.295 |
| 7372.3677 | 7362.3090 | 7357.8981 | 7355.4940 | 1.41 | 7348.9456 | 7348.840 |
| 7908.8464 | 7893.3931 | 7887.7663 | 7885.1085 | 1.94 | 7880.1286 | 7880.084 |
| 12831.2888 | 12784.9811 | 12768.5793 | 12760.9513 | 2.01 | 12747.2677 | 12746.802 |
| 13137.3479 | 13095.2059 | 13078.7328 | 13070.4722 | 1.73 | 13052.7434 | 13051.758 |
| 14968.4108 | 14926.3074 | 14911.1135 | 14903.9436 | 1.96 | 14890.7177 | 14890.114 |
| $\nu = 0.49$ | | | | | | |
| 3081.8429 | 3059.1117 | 3048.8806 | 3043.1623 | 1.32 | 3026.3099 | 3025.120 |
| 8032.0292 | 7997.6323 | 7981.9373 | 7973.0925 | 1.29 | 7946.4129 | 7945.193 |
| 8077.3101 | 8060.6008 | 8054.6502 | 8051.8958 | 2.01 | 8046.9569 | 8046.967 |
| 12789.6444 | 12733.3815 | 12709.3393 | 12696.4308 | 1.48 | 12663.2748 | 12660.250 |
| 13234.2998 | 13193.7694 | 13179.4864 | 13172.8689 | 2.03 | 13161.1898 | 13161.057 |
| 15754.1992 | 15663.4991 | 15628.0896 | 15610.2044 | 1.73 | 15572.0923 | 15567.043 |
| $\nu = 0.5$ | | | | | | |
| 3096.0660 | 3071.3635 | 3060.2058 | 3053.9532 | 1.31 | 3035.3659 | 3034.018 |
| 8090.3425 | 8052.5697 | 8035.2770 | 8025.5048 | 1.28 | 7995.7653 | 7994.348 |
| 8098.9778 | 8081.7157 | 8075.5863 | 8072.7571 | 2.01 | 8067.6493 | 8067.720 |
| 12775.5424 | 12716.6767 | 12691.3138 | 12677.6156 | 1.45 | 12641.4334 | 12638.546 |
| 13268.7664 | 13228.2525 | 13213.9786 | 13207.3680 | 2.03 | 13195.6921 | 13195.563 |
| 15792.0288 | 15697.3630 | 15660.1027 | 15641.1543 | 1.70 | 15599.7755 | 15594.866 |

## 5.2 2D square with discontinuous Lamé parameters

In this experiment we again consider the unit square $\Omega := (0, 1)^2$, but this time we take a Young's modulus such that the Lamé parameters are discontinuous. More precisely, we subdivide $\Omega$ into three regions $\Omega := \Omega_1 \cup \Omega_2 \cup \Omega_3$, given by,

$$\Omega_1 := (0, 1/3) \times (0, 1), \quad \Omega_2 := (1/3, 2/3) \times (0, 1), \quad \Omega_3 := (2/3, 1) \times (0, 1),$$

such that the Young's modulus is defined by

$$E(x) = \begin{cases} 2, & \text{if } x \in \Omega_1, \\ 1, & \text{if } x \in \Omega_2, \\ 3, & \text{if } x \in \Omega_3. \end{cases}$$

**Table 3** Test 5.1. Lowest computed eigenvalues for the lowest order Taylor-Hood family and different values of $\nu$.

| $N = 20$ | $N = 30$ | $N = 40$ | $N = 50$ | Order | $\sqrt{\widehat{\kappa}_{extr}}$ | [22] |
|---|---|---|---|---|---|---|
| | | | $\nu = 0.35$ | | | |
| 2947.9433 | 2946.3921 | 2945.7107 | 2945.3380 | 1.41 | 2944.3200 | 2944.295 |
| 7353.0241 | 7351.2280 | 7350.4365 | 7350.0038 | 1.40 | 7348.8078 | 7348.840 |
| 7880.6474 | 7880.4027 | 7880.3240 | 7880.2879 | 2.26 | 7880.2343 | 7880.084 |
| 12747.5800 | 12747.4026 | 12747.3597 | 12747.3431 | 3.04 | 12747.3271 | 12746.802 |
| 13059.0437 | 13055.8615 | 13054.5253 | 13053.8104 | 1.53 | 13052.0477 | 13051.758 |
| 14891.6919 | 14891.1322 | 14890.9288 | 14890.8270 | 1.91 | 14890.6395 | 14890.114 |
| | | | $\nu = 0.49$ | | | |
| 3036.8461 | 3032.3233 | 3030.2238 | 3029.0275 | 1.25 | 3025.2710 | 3025.120 |
| 7963.1337 | 7956.1517 | 7952.8860 | 7951.0235 | 1.23 | 7945.0430 | 7945.193 |
| 8047.2590 | 8047.1328 | 8047.1054 | 8047.0967 | 3.41 | 8047.0887 | 8046.967 |
| 12680.2906 | 12672.3064 | 12668.6743 | 12666.6299 | 1.30 | 12660.4821 | 12660.250 |
| 13161.3264 | 13161.1886 | 13161.1630 | 13161.1555 | 3.83 | 13161.1499 | 13161.057 |
| 15583.8476 | 15577.3533 | 15574.4389 | 15572.8137 | 1.34 | 15568.0999 | 15567.043 |
| | | | $\nu = 0.5$ | | | |
| 3046.7873 | 3041.8988 | 3039.6212 | 3038.3196 | 1.24 | 3034.1970 | 3034.018 |
| 8014.1126 | 8006.4753 | 8002.8886 | 8000.8375 | 1.22 | 7994.1937 | 7994.348 |
| 8068.0073 | 8067.8864 | 8067.8616 | 8067.8543 | 3.59 | 8067.8479 | 8067.720 |
| 12660.2310 | 12651.6456 | 12647.7223 | 12645.5075 | 1.29 | 12638.7963 | 12638.546 |
| 13195.8533 | 13195.7132 | 13195.6869 | 13195.6789 | 3.78 | 13195.6730 | 13195.563 |
| 15613.2772 | 15606.0211 | 15602.7442 | 15600.9105 | 1.33 | 15595.5636 | 15594.866 |

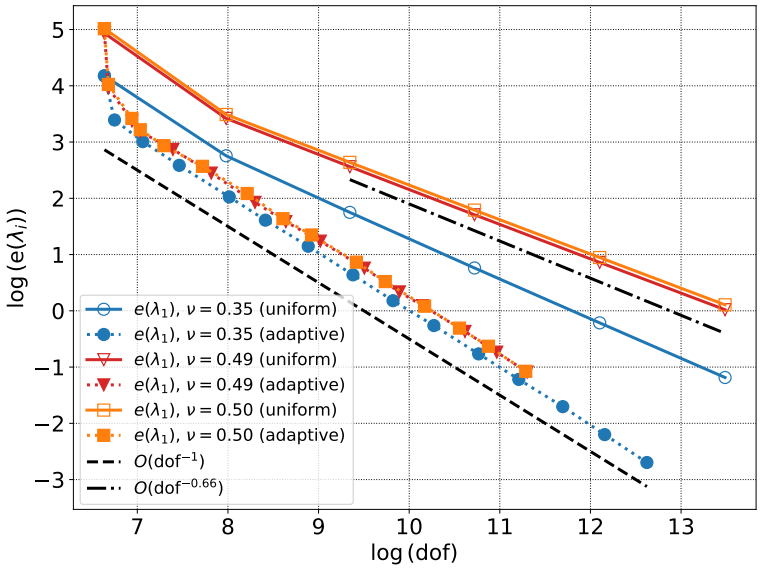


**Fig. 1** Test 5.1. Error curves obtained from the adaptive algorithm in the bottom-clamped square domain compared with the lines $\mathcal{O}(\mathtt{dof}^{-0.66})$ and $\mathcal{O}(\mathtt{dof}^{-1})$.

The material density is assumed to be 1. This implies that both $\mu$ and $\lambda$ are discontinuous functions. In Figure 4 we can observe the division of domain $\Omega$, and the triangulation for this case. Here, the mesh size is given by $h \approx 1/N$, where $N$ is the mesh level.

Table 4 presents the result for the mini-element family. Here, we observe that a quadratic rate of convergence is attained for all the considered values of $\nu = 0.35$. However, for the other cases, the first eigenmode is affected by the pressure discontinuity and behaves like $\mathcal{O}(h^{1.7})$. This contrast with the results when using the Taylor-hood family, where a quadratic rate is observe for the first eigenmode in all cases. However, the fifth eigenmode also behaves like $\mathcal{O}(h^{1.7})$. Since we are dealing with discontinuous Lamé parameters, Taylor-Hood elements are not capable of giving more than

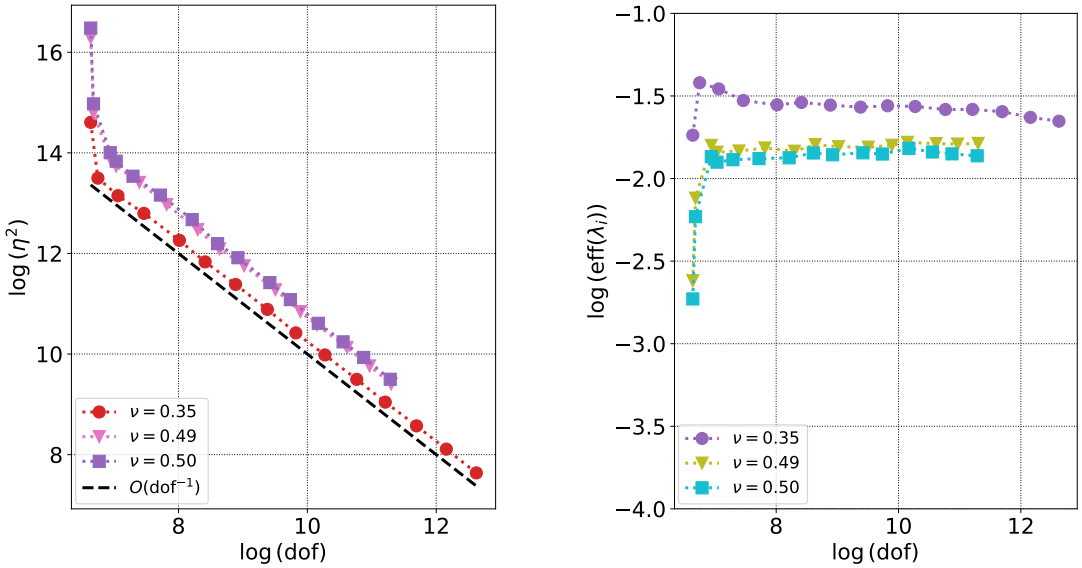


**Fig. 2** Test 5.1. Estimator and efficiency curves obtained from the adaptive algorithm in the bottom-clamped square domain for different values of $\nu$.

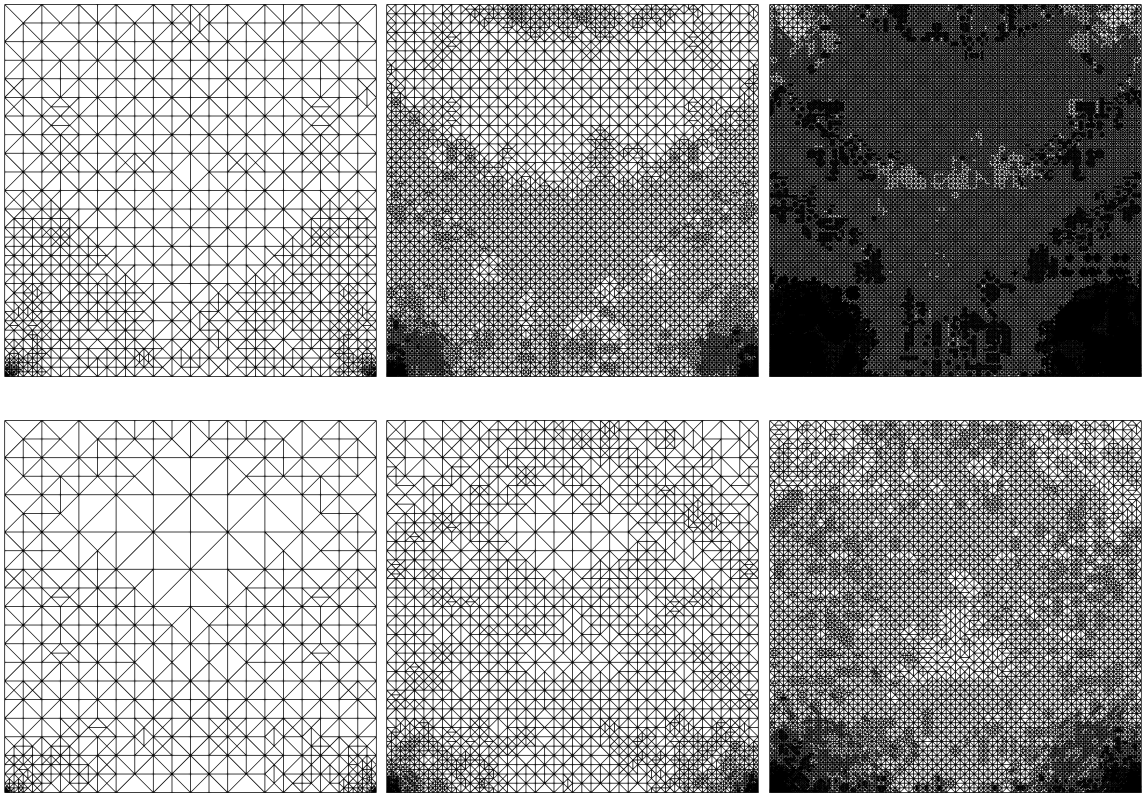

**Fig. 3** Test 5.1. Intermediate meshes of the unit square domain obtained with the adaptive algorithm and different values of $\nu$. Top row: Meshes with 7229, 47399 and 303396 dofs with $\eta = 0.35$. Bottom row: Meshes with 3686, 16917 and 79705 dofs with $\eta = 0.5$.

$\mathcal{O}(h^2)$. We also present the eigenmodes for the velocity fields and pressure modes in Figures 5 and

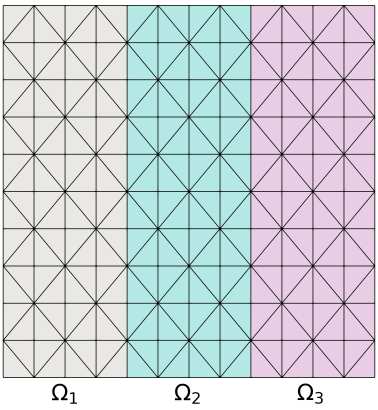


**Fig. 4** Test 5.2. Sample mesh of the domain $\Omega$ subdivided in $\Omega_i$, $i = 1, 2, 3$ subdomains.

6 for $\nu = 0.35$ and $\nu = 0.49999$, respectively. It is observed that the flow distributes according to the values of $E$, showing high velocities around the center of the geometry. In order to observe the pressure jumps, we have projected the pressure into the lowest discontinuous Lagrange family of elements $\mathbb{P}_0(\mathcal{T}_h)$. One can also compute the respective 2D contour plot.

**Table 4** Test 5.2. Lowest computed eigenvalues using the mini-element family for different values of $\nu$ and discontinuous $\mu$ and $\lambda$.

| $N = 20$ | $N = 30$ | $N = 40$ | $N = 50$ | Order | $\sqrt{\widehat{\kappa}_{extr}}$ |
|---|---|---|---|---|---|
| | | $\nu = 0.35$ | | | |
| 5.2021 | 5.1924 | 5.1883 | 5.1869 | 2.01 | 5.1838 |
| 6.0415 | 6.0167 | 6.0063 | 6.0023 | 2.00 | 5.9943 |
| 6.0956 | 6.0851 | 6.0806 | 6.0788 | 1.91 | 6.0751 |
| 7.8128 | 7.7540 | 7.7310 | 7.7219 | 2.12 | 7.7057 |
| 7.8784 | 7.8445 | 7.8305 | 7.8252 | 2.04 | 7.8148 |
| | | $\nu = 0.49$ | | | |
| 5.8413 | 5.8145 | 5.8025 | 5.7974 | 1.75 | 5.7857 |
| 7.0706 | 7.0224 | 7.0016 | 6.9937 | 1.93 | 6.9767 |
| 7.3501 | 7.2883 | 7.2630 | 7.2519 | 1.95 | 7.2311 |
| 8.6728 | 8.5649 | 8.5216 | 8.5036 | 2.03 | 8.4706 |
| 9.0578 | 8.9419 | 8.8960 | 8.8759 | 2.02 | 8.8403 |
| | | $\nu = 0.49999$ | | | |
| 5.8308 | 5.8037 | 5.7912 | 5.7859 | 1.70 | 5.7732 |
| 7.1643 | 7.1124 | 7.0902 | 7.0818 | 1.96 | 7.0641 |
| 7.3614 | 7.2979 | 7.2716 | 7.2599 | 1.91 | 7.2375 |
| 8.7113 | 8.5990 | 8.5540 | 8.5352 | 2.03 | 8.5009 |
| 9.0746 | 8.9554 | 8.9079 | 8.8868 | 2.00 | 8.8494 |

## 5.3 2D L-shaped domain

In this experiment we put to the test the performance of the estimator when the domain present two types of singularities and also have discontinuous Lamé parameters. The domain in consideration is the L-shape domain $\Omega := (-1, 1)^2 \setminus ((0, 1) \times (-1, 0))$. More precisely, we consider the domain to be free of stress at $y = -1$ and $x = 1$, and clamped in the rest of the boundary. The Lamé parameters

**Table 5** Test 5.2. Lowest computed eigenvalues using the lowest order Taylor-Hood family for different values of $\nu$ and discontinuous $\mu$ and $\lambda$.

| $N = 20$ | $N = 30$ | $N = 40$ | $N = 50$ | Order | $\sqrt{\widehat{\kappa}_{extr}}$ |
|---|---|---|---|---|---|
| | | $\nu = 0.35$ | | | |
| 5.1820 | 5.1836 | 5.1842 | 5.1844 | 2.20 | 5.1848 |
| 5.9934 | 5.9945 | 5.9949 | 5.9951 | 2.28 | 5.9953 |
| 6.0687 | 6.0723 | 6.0739 | 6.0745 | 1.84 | 6.0759 |
| 7.6973 | 7.7013 | 7.7030 | 7.7037 | 1.96 | 7.7050 |
| 7.8064 | 7.8111 | 7.8131 | 7.8139 | 1.88 | 7.8157 |
| | | $\nu = 0.49$ | | | |
| 5.7859 | 5.7880 | 5.7888 | 5.7890 | 2.28 | 5.7895 |
| 6.9730 | 6.9762 | 6.9774 | 6.9779 | 2.20 | 6.9787 |
| 7.2263 | 7.2303 | 7.2320 | 7.2326 | 1.99 | 7.2340 |
| 8.4596 | 8.4659 | 8.4685 | 8.4696 | 2.01 | 8.4716 |
| 8.8327 | 8.8374 | 8.8396 | 8.8405 | 1.71 | 8.8427 |
| | | $\nu = 0.49999$ | | | |
| 5.7740 | 5.7761 | 5.7770 | 5.7772 | 2.28 | 5.7777 |
| 7.0608 | 7.0636 | 7.0647 | 7.0651 | 2.18 | 7.0658 |
| 7.2336 | 7.2377 | 7.2394 | 7.2400 | 2.01 | 7.2413 |
| 8.4901 | 8.4964 | 8.4990 | 8.5000 | 2.01 | 8.5020 |
| 8.8426 | 8.8473 | 8.8496 | 8.8504 | 1.71 | 8.8526 |

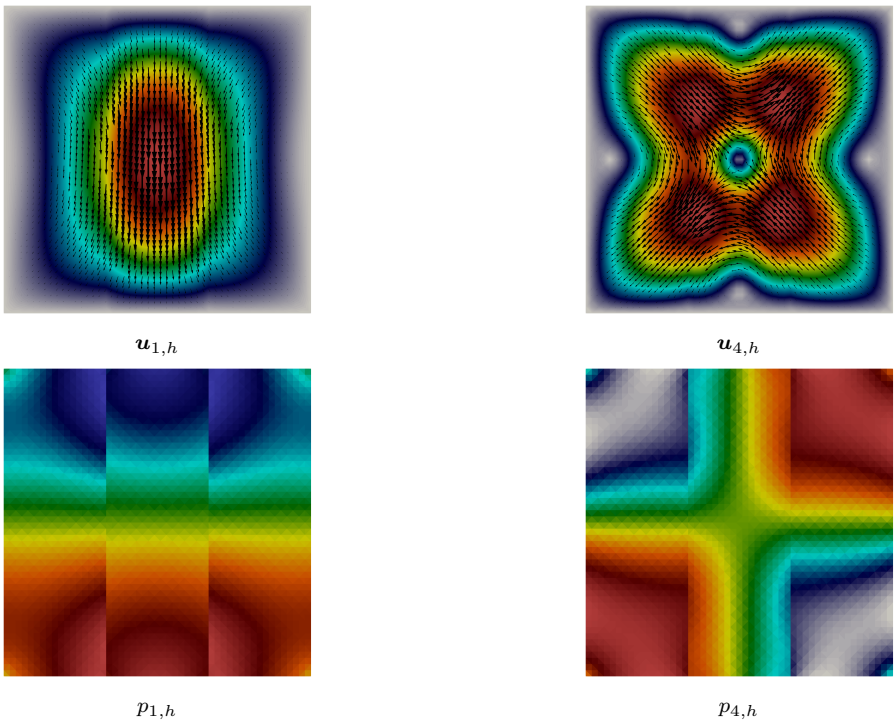


**Fig. 5** Test 5.2. Displacement/velocity fields and pressure surface plot for the first and fourth eigenmodes for $\nu = 0.35$ and discontinuous $\mu$ and $\lambda$.

for this experiments depend on the Young modulus, which is given by

$$E(x) = \begin{cases} \sqrt{x^2 + y^2 + 4}, & \text{if } x \in \Omega_1, \\ \sqrt{x^2 + y^2 + 2}, & \text{if } x \in \Omega_2, \\ \sqrt{x^2 + y^2 + 4}, & \text{if } x \in \Omega_3. \end{cases}$$

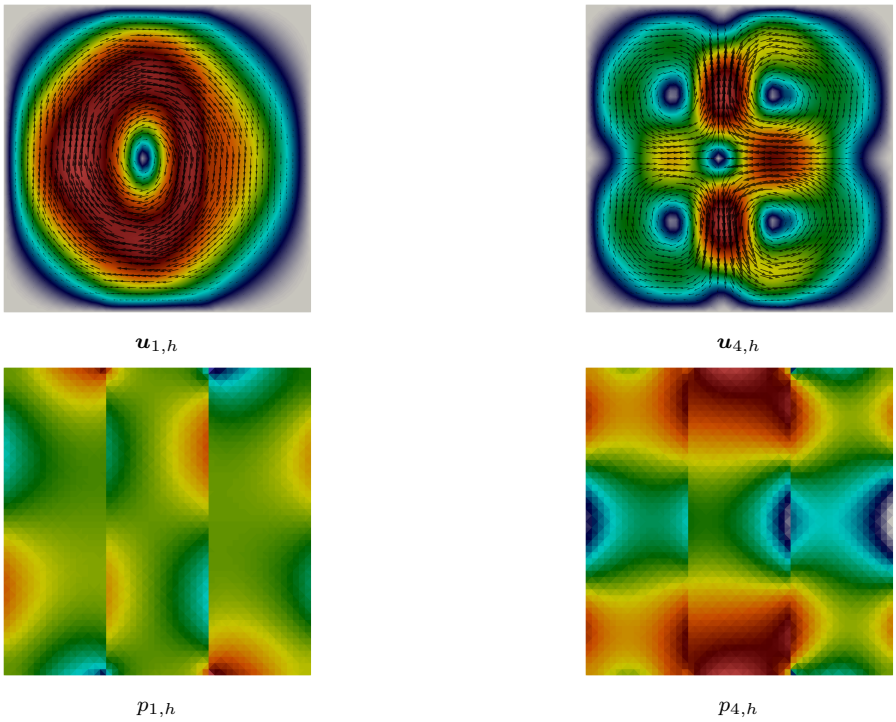


**Fig. 6** Test 5.2. Displacement/velocity fields and pressure surface plot for the first and fourth eigenmodes for $\nu = 0.49999$ and discontinuous $\mu$ and $\lambda$.

A sample of the initial mesh and the subdomains is depicted in Figure 7. Note that the domain contains a singularity at $(x, y) = (0, 0)$, followed by the points where boundary conditions change from Neumann to Dirichlet type. Also, the Young modulus present discontinuities along the boundary of each subdomain. Hence, suboptimality with uniform refinements is assured. The exact lowest computed eigenvalues for each value of $\nu$ are given in Table 6 below.

| $\nu$ | $\sqrt{\widehat{\kappa}_1}$ |
|---|---|
| 0.35 | 2.66229608762752 |
| 0.49 | 2.56684460283184 |
| 0.5 | 2.56098604836068 |

**Table 6** Test 5.3. Reference lowest computed eigenvalues for different values of $\nu$.

Evidence of uniform and adaptive refinements are observed in Figure 8, where suboptimal rate of convergence is observed if uniform refinements are used. Indeed, the convergence rate for $\nu = 0.35$ is about $\mathcal{O}(\texttt{dof}^{-0.48})$, while $\mathcal{O}(\texttt{dof}^{-0.44})$ is observed for $\nu = 0.49$ and $\nu = 0.50$. For the adaptive refinements, an experimental rate $\mathcal{O}(\texttt{dof}^{-1.01})$ was observed for $\nu = 0.35$ and $\nu = 0.49$, whereas $\mathcal{O}(\texttt{dof}^{-0.99})$ was obtained for $\nu = 0.5$. On Figure 9 we observe that the estimator behaves similar to $\mathcal{O}(h^2)$ for all the selected values of $\nu$, obtaining a bounded efficiency between 0.0036 and 0.0041. Figure 10 portray different meshes obtained in the adaptive refinements. It notes that the refinements are concentrated in the re-entrant corner, the four points where Dirichlet boundary changes to Neumann, and also on the subdomains boundary, where the physical parameters have jumps. Similar to the square domain case, the number of elements marked for $\nu = 0.35$ is greater than those marked with $\nu = 0.50$. Figure 11 present the corresponding lowest computed velocity and pressure eigenmodes, where we observe very small difference in the field $\boldsymbol{u}_{1,h}$, and evident discontinuities for the pressure contour plot in the subdomain boundaries are observed.

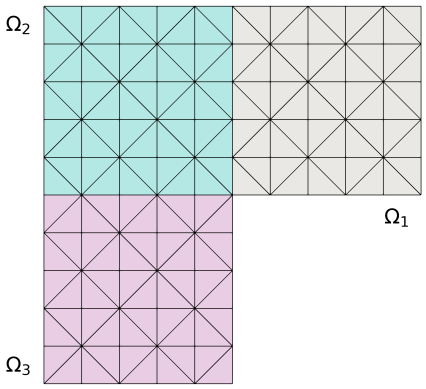


**Fig. 7** Test 5.3. Initial mesh of the domain $\Omega$ subdivided in $\Omega_i$, $i = 1, 2, 3$ subdomains.

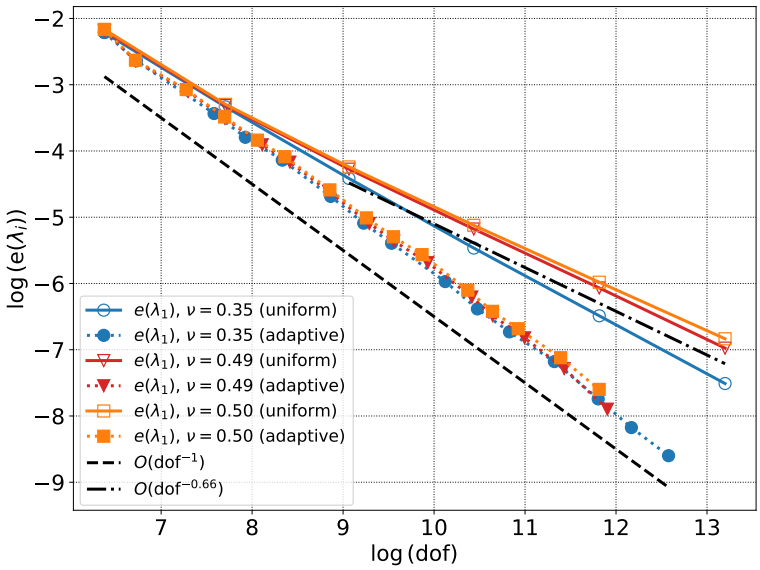


**Fig. 8** Example 5.3. Error curves obtained from the adaptive algorithm in the Lshaped domain compared with the lines $\mathcal{O}(\texttt{dof}^{-0.66})$ and $\mathcal{O}(\texttt{dof}^{-1})$.

## 5.4 A three dimensional test

Now we report some results for a three dimensional test. the domain under consideration is the unit cube $\Omega := (0, 1)^3$. For simplicity, because of the high computational cost when a 3D test is performed for eigenvalue problems, we focus on the lowest order finite elements. The boundary conditions for this test is the same as Test 5.1, namely, we assume that the cube is fixed at the bottom and free of stress in the rest of its geometry. For simplicity, we consider $E = \rho = 1$.

Tables 7 and 8 shows the convergence behaviour when computing the first four eigenmodes. It notes that since we have edges singularities along the bottom facet of the cube, the convergence rate behaves like $\mathcal{O}(h^r)$, with $r \geq 1.36$ for the elastic case, whereas $r \geq 1.2$ for the limit Stokes scenario. We also note that both methods deals with the singularity in a slightly different manner. For instance, a quadratic order is observed in the fourth eigenvalue when Taylor-Hood is used. However, this is still not optimal for this family. On the other hand, suboptimal convergence is also observe for this eigenvalue for the mini-element family, where the rate behaves like $\mathcal{O}(h^{1.7})$ for the three $\nu$ scenarios. Finally, we present in Figure 13 the first and fourth lowest computed eigenmodes from Table 8. We depict the

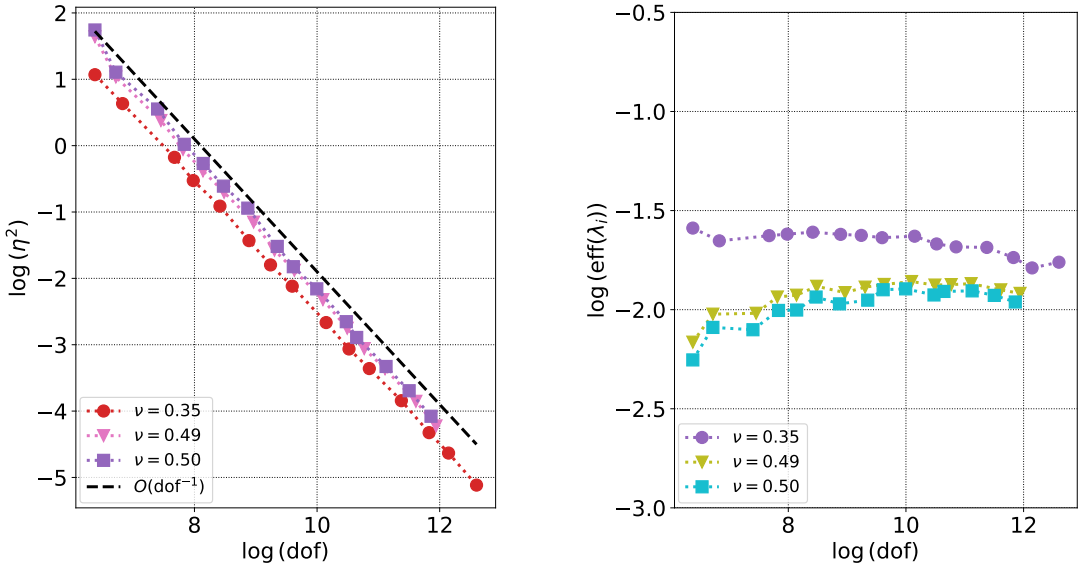


**Fig. 9** Example 5.3. Estimator and efficiency curves obtained from the adaptive algorithm in the Lshaped domain with different values of $\nu$.

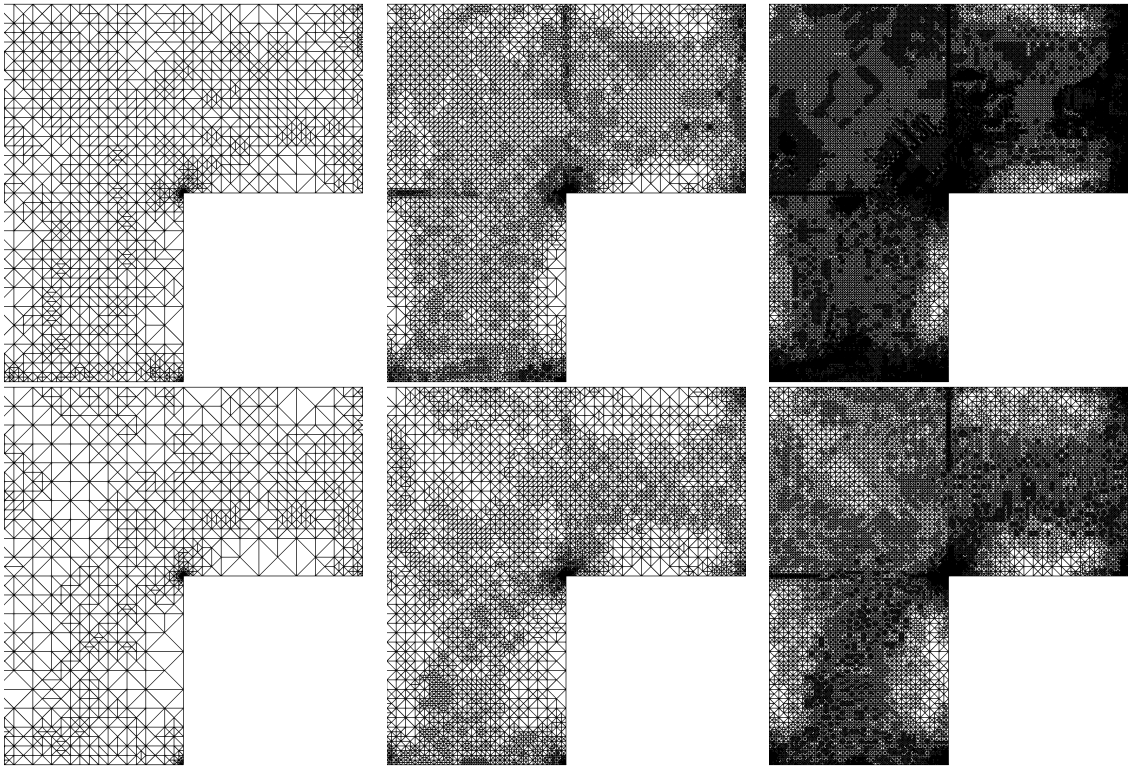

**Fig. 10** Test 5.3. Intermediate meshes of the Lshaped domain obtained with the adaptive algorithm and different values of $\nu$. Top row: Meshes with 10163, 50455 and 289949 dofs with $\eta = 0.35$. Bottom row: Meshes with 7006, 31911 and 135217 dofs with $\eta = 0.5$.

displacement ($\nu = 0.35$) or the velocity field ($\nu = 0.5$) accompanied with their corresponding pressures surface plot.

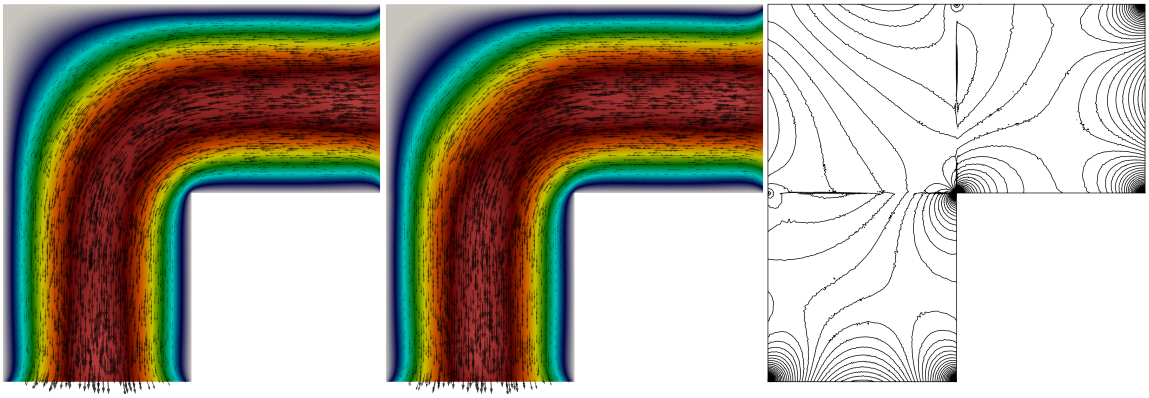

**Fig. 11** Test 5.3. Velicity fields for the first computed eigenfrequency for $\nu = 0.35$ (left) and $\nu = 0.50$ (right) together with the singular pressure contour plot, similar for both cases.

For the adaptive refinement, we consider the first eigenvalue. Note that this choice characterized by the fact this eigenvalue has multiplicity 2, hence it is beyond the theoretical results since we have no control over the distance function between this two values on the a posteriori analysis. However, as we observe in Figure 14, an optimal rate is obtained for 10 iterations of the adaptive algorithm. For instance, a rate of $\mathcal{O}(\texttt{dof}^{-0.66})$ was observed for the last 4 refinements. Evidence of the adaptive meshes are depicted in Figure 12, where we observe that the refinements are performed near the edges where the boundary condition changes. On Figure 13 we observe that the first eigenmode for each $\nu$ has pressure singularities precisely on the zones where the adaptive algorithm perform the refinements. We also present the fourth eigenmode, which shows a high pressure gradient near the bottom edges, resulting in the suboptimal behavior observed in Tables 7 and 8.

**Table 7** Test 5.4. Lowest computed eigenvalues in the unit cube domain with mixed boundary conditions using the mini-element family for different values of $\nu$.

| $N = 10$ | $N = 15$ | $N = 20$ | $N = 25$ | Order | $\sqrt{\widehat{\kappa}_{extr}}$ |
|---|---|---|---|---|---|
| $\nu = 0.35$ | | | | | |
| 0.6794 | 0.6736 | 0.6711 | 0.6698 | 1.51 | 0.6666 |
| 0.6830 | 0.6753 | 0.6721 | 0.6705 | 1.59 | 0.6666 |
| 0.9234 | 0.9066 | 0.9002 | 0.8972 | 1.85 | 0.8911 |
| 1.6203 | 1.6138 | 1.6110 | 1.6094 | 1.41 | 1.6052 |
| 1.7831 | 1.7661 | 1.7596 | 1.7564 | 1.77 | 1.7496 |
| $\nu = 0.49$ | | | | | |
| 0.6946 | 0.6842 | 0.6796 | 0.6770 | 1.34 | 0.6696 |
| 0.6985 | 0.6861 | 0.6807 | 0.6777 | 1.41 | 0.6697 |
| 0.8833 | 0.8665 | 0.8600 | 0.8567 | 1.77 | 0.8500 |
| 1.6838 | 1.6670 | 1.6597 | 1.6557 | 1.42 | 1.6450 |
| 1.7479 | 1.7282 | 1.7204 | 1.7166 | 1.72 | 1.7082 |
| $\nu = 0.5$ | | | | | |
| 0.6974 | 0.6862 | 0.6812 | 0.6784 | 1.33 | 0.6702 |
| 0.7015 | 0.6882 | 0.6823 | 0.6791 | 1.40 | 0.6703 |
| 0.8811 | 0.8641 | 0.8575 | 0.8543 | 1.75 | 0.8473 |
| 1.6912 | 1.6728 | 1.6649 | 1.6605 | 1.42 | 1.6488 |
| 1.7464 | 1.7262 | 1.7182 | 1.7143 | 1.71 | 1.7055 |

## 5.5 Robustness test on 2D and 3D geometries

In this last experiment we assess the robustness of our estimator in two and three dimensions. More precisely, we consider the unit square $\Omega := (0,1)^2$ and the unit cube domain $\Omega := (0,1)^3$, respectively.

**Table 8** Test 5.4. Lowest computed eigenvalues in the unit cube domain with mixed boundary conditions using the Taylor-Hood family for different values of $\nu$.

| $N = 10$ | $N = 15$ | $N = 20$ | $N = 25$ | Order | $\sqrt{\widehat{\kappa}_{extr}}$ |
|---|---|---|---|---|---|
| | | $\nu = 0.35$ | | | |
| 0.6680 | 0.6673 | 0.6670 | 0.6669 | 1.42 | 0.6664 |
| 0.6681 | 0.6674 | 0.6671 | 0.6669 | 1.47 | 0.6664 |
| 0.8920 | 0.8916 | 0.8915 | 0.8914 | 2.28 | 0.8914 |
| 1.6073 | 1.6064 | 1.6060 | 1.6057 | 1.39 | 1.6051 |
| 1.7509 | 1.7505 | 1.7503 | 1.7502 | 2.44 | 1.7502 |
| | | $\nu = 0.49$ | | | |
| 0.6730 | 0.6715 | 0.6708 | 0.6704 | 1.27 | 0.6692 |
| 0.6731 | 0.6716 | 0.6709 | 0.6705 | 1.32 | 0.6693 |
| 0.8513 | 0.8508 | 0.8506 | 0.8505 | 1.85 | 0.8502 |
| 1.6493 | 1.6471 | 1.6461 | 1.6454 | 1.20 | 1.6434 |
| 1.7100 | 1.7094 | 1.7091 | 1.7090 | 1.99 | 1.7088 |
| | | $\nu = 0.5$ | | | |
| 0.6738 | 0.6723 | 0.6715 | 0.6711 | 1.26 | 0.6698 |
| 0.6740 | 0.6723 | 0.6716 | 0.6711 | 1.31 | 0.6699 |
| 0.8487 | 0.8481 | 0.8479 | 0.8478 | 1.83 | 0.8476 |
| 1.6532 | 1.6509 | 1.6498 | 1.6491 | 1.18 | 1.6469 |
| 1.7074 | 1.7067 | 1.7065 | 1.7064 | 1.96 | 1.7061 |

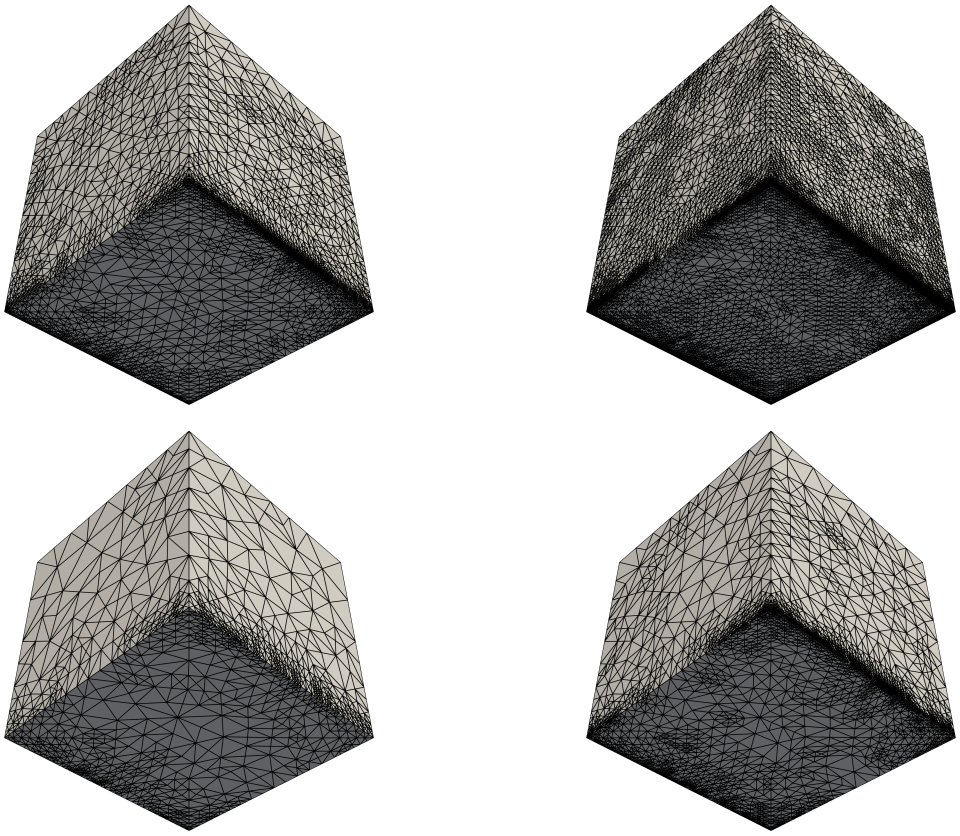

**Fig. 12** Test 5.4. Bottom view of intermediate meshes of the bottom-clamped unit cube domain obtained with the adaptive algorithm and different values of $\nu$. Top row: Meshes with 473830 and 2146942 dofs with $\eta = 0.35$. Bottom row: Meshes with 97753 and 314288 dofs with $\eta = 0.5$

We will give different constant values to Young's modulus $E$ in order to observe the behavior of `eff`. Let us note that from (2.3) we have $\mu$ and $\lambda$ we have that $\mu = E/2$ and $\lambda = \frac{2\mu\nu}{1-2\nu}$. For this experiment,

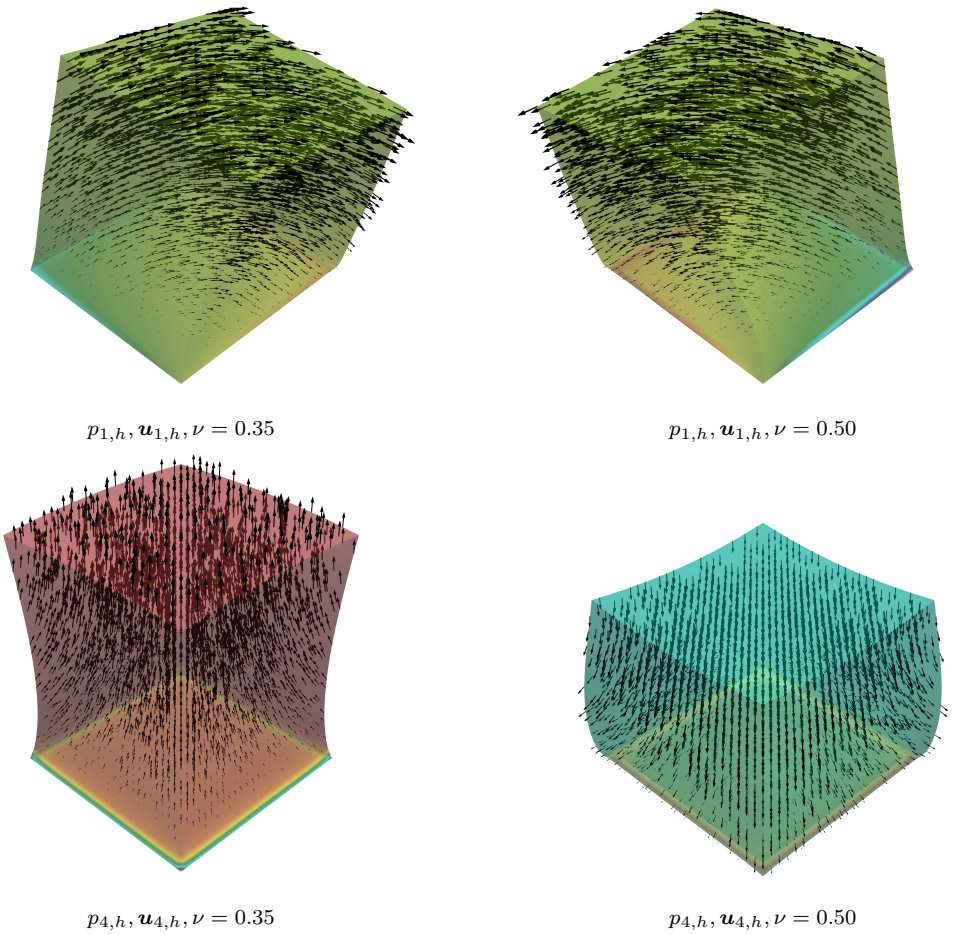


**Fig. 13** Test 5.4. Top view of the unit cube 3D representation of the displacement/velocity field, together with the corresponding pressure surface plots for the first and fourth lowest order eigenmodes with $\nu = 0.35$ and $\nu = 0.50$.

$\rho$ is set to be 1. The boundary conditions for this test are the same as Section 5.1 for the square domain and Section 5.4 for the cube domain, i.e., we assume that both geometries are fixed at the bottom plane and free of stress in the rest of the facets. Because of the results obtained in previous sections, it is enough to the test the estimator using uniform refinements.

The extrapolated values for this experiment are calculated from a reference value for each value of $\nu$. More precisely, in each test we have the following extrapolated values for $E = 10^j, j = 1, 2, 3....$

| | Square domain | Cube domain |
|---|---|---|
| $\nu$ | $\widehat{\kappa}_1$ | $\widehat{\kappa}_1$ |
| 0.35 | $0.46355423498481496 \cdot E$ | $0.444317882233217 \cdot E$ |
| 0.49 | $0.48938358373431 \cdot E$ | $0.44833605908518 \cdot E$ |
| 0.5 | $0.492273855811713 \cdot E$ | $0.44915941661888 \cdot E$ |

**Table 9** Test 5.5. Reference lowest computed eigenvalues for different values of $\nu$ and $E = 10^j, j = 1, 2, 3...$ .

Although uniform refinements have been used, giving a convergence like $\mathcal{O}(h^{1.32})$, the estimator remains robust with respect to the physical parameters. In fact, in Table 10 we observe different efficiency indexes obtained by manipulating the value of $E$ with several powers of 10. For each value of $\nu$, properly bounded efficiency indexed are obtained, which are shown to be independent of the

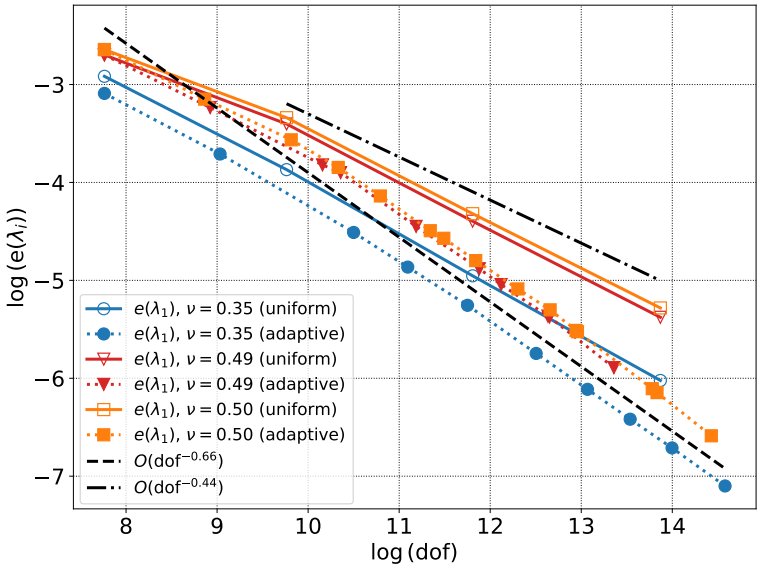


**Fig. 14** Example 5.3. Error curves obtained from the adaptive algorithm in the unit cube domain compared with the lines $\mathcal{O}(\texttt{dof}^{-0.45})$ and $\mathcal{O}(\texttt{dof}^{-0.66})$.

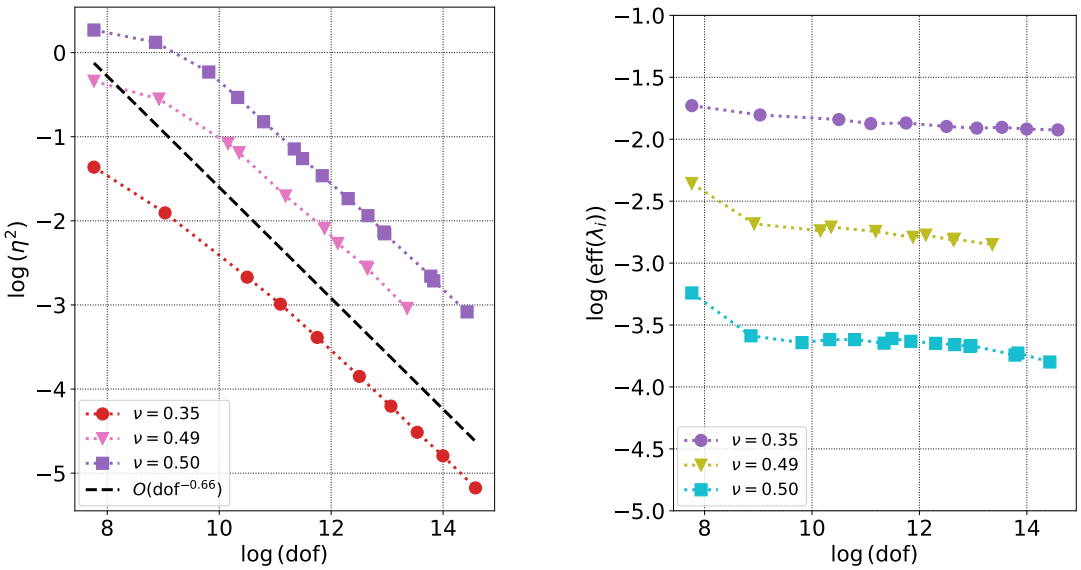


**Fig. 15** Example 5.3. Estimator and efficiency curves obtained from the adaptive algorithm in the unit cube domain with different values of $\nu$.

value of $E$, even in the limit $\nu = 0.5$. We remark that similar values were obtained when testing with $E = 10^{-j}, j = 0, 1, 2$, confirming the robustness of the proposed estimator.

**Acknowledgements** This work was advanced during the ICOSAHOM 2023 conference, Seoul, Korea. AK was partially supported by the Sponsored Research & Industrial Consultancy (SRIC), Indian Institute of Technology Roorkee, India through the faculty initiation grant MTD/FIG/100878; by SERB MATRICS grant MTR/2020/000303; by SERB Core research grant CRG/2021/002569; FL was partially supported by DIUBB through project 2120173 GI/C Universidad del Bío-Bío and ANID-Chile through FONDECYT project 11200529 (Chile). DM was partially supported by the National Agency for Research and Development, ANID-Chile through project Anillo of Computational Mathematics for Desalination Processes ACT210087, by FONDECYT project 1220881, and by project Centro de Modelamiento Matemático (CMM), FB210005, BASAL funds for centers of excellence. JV was partially supported by the National

| | $\nu = 0.35$ | | | $\nu = 0.49$ | | | $\nu = 0.50$ | | |
|---|---|---|---|---|---|---|---|---|---|
| Unit square domain $\Omega = (0,1)^2$ | | | | | | | | | |
| dof | eff($\widehat{\kappa}_1$) | | | eff($\widehat{\kappa}_1$) | | | eff($\widehat{\kappa}_1$) | | |
| 84 | 1.94e-01 | 1.94e-01 | 1.94e-01 | 9.05e-02 | 9.05e-02 | 9.05e-02 | 8.25e-02 | 8.25e-02 | 8.25e-02 |
| 208 | 1.96e-01 | 1.96e-01 | 1.96e-01 | 8.95e-02 | 8.95e-02 | 8.95e-02 | 8.07e-02 | 8.07e-02 | 8.07e-02 |
| 624 | 2.01e-01 | 2.01e-01 | 2.01e-01 | 9.07e-02 | 9.07e-02 | 9.07e-02 | 8.12e-02 | 8.12e-02 | 8.12e-02 |
| 2128 | 2.07e-01 | 2.07e-01 | 2.07e-01 | 9.28e-02 | 9.28e-02 | 9.28e-02 | 8.27e-02 | 8.27e-02 | 8.27e-02 |
| 7824 | 2.10e-01 | 2.10e-01 | 2.10e-01 | 9.42e-02 | 9.42e-02 | 9.42e-02 | 8.39e-02 | 8.39e-02 | 8.39e-02 |
| 29968 | 2.11e-01 | 2.11e-01 | 2.11e-01 | 9.44e-02 | 9.44e-02 | 9.44e-02 | 8.41e-02 | 8.41e-02 | 8.41e-02 |
| Unit cube domain $\Omega = (0,1)^3$ | | | | | | | | | |
| dof | eff($\widehat{\kappa}_1$) | | | eff($\widehat{\kappa}_1$) | | | eff($\widehat{\kappa}_1$) | | |
| 2351 | 6.82e-01 | 6.82e-01 | 6.82e-01 | 1.77e-01 | 1.77e-01 | 1.77e-01 | 1.42e-01 | 1.42e-01 | 1.42e-01 |
| 17384 | 6.45e-01 | 6.45e-01 | 6.45e-01 | 1.02e-01 | 1.02e-01 | 1.02e-01 | 7.76e-02 | 7.76e-02 | 7.76e-02 |
| 134172 | 7.73e-01 | 7.73e-01 | 7.73e-01 | 1.04e-01 | 1.04e-01 | 1.04e-01 | 7.84e-02 | 7.84e-02 | 7.84e-02 |
| 1055284 | 8.21e-01 | 8.21e-01 | 8.21e-01 | 9.86e-02 | 9.86e-02 | 9.86e-02 | 7.32e-02 | 7.32e-02 | 7.32e-02 |
| $E$ | 10 | $10^2$ | $10^4$ | 10 | $10^2$ | $10^4$ | 10 | $10^2$ | $10^4$ |

**Table 10** Test 5.5. Efficiency indexes for different values of $\nu$ and $E$ on the unit square and unit cube domain.

Agency for Research and Development, ANID-Chile through project Anillo of Computational Mathematics for Desalination Processes ACT210087, by FONDECYT Postdoctorado project 3230302, and by project Centro de Modelamiento Matemático (CMM), FB210005, BASAL funds for centers of excellence.

## References


1. M. Ainsworth and J. T. Oden, *A posteriori error estimation in finite element analysis*, Pure and Applied Mathematics (New York), Wiley-Interscience [John Wiley & Sons], New York, 2000.
2. M. S. Alnæs, J. Blechta, J. Hake, A. Johansson, B. Kehlet, A. Logg, C. Richardson, J. Ring, M. E. Rognes, and G. N. Wells, *The fenics project version 1.5*, Archive of Numerical Software, 3 (2015).
3. L. Alzaben, F. Bertrand, and D. Boffi, *On the spectrum of an operator associated with least-squares finite elements for linear elasticity*, Comput. Methods Appl. Math., 22 (2022), pp. 511–528.
4. I. Babuška and J. Osborn, *Eigenvalue problems*, Handb. Numer. Anal., II, North-Holland, Amsterdam, 1991.
5. F. Bertrand and D. Boffi, *Least-squares formulations for eigenvalue problems associated with linear elasticity*, Comput. Math. Appl., 95 (2021), pp. 19–27.
6. F. Bertrand, D. Boffi, and R. Ma, *An adaptive finite element scheme for the Hellinger–Reissner elasticity mixed eigenvalue problem*, Computational Methods in Applied Mathematics, 21 (2021), pp. 501–512.
7. D. Boffi, *Finite element approximation of eigenvalue problems*, Acta Numer., 19 (2010), pp. 1–120.
8. D. Boffi, F. Brezzi, and M. Fortin, *Mixed finite element methods and applications*, vol. 44 of Springer Series in Computational Mathematics, Springer, Heidelberg, 2013.
9. A. Ern and J.-L. Guermond, *Theory and practice of finite elements*, vol. 159 of Applied Mathematical Sciences, Springer-Verlag, New York, 2004.
10. E. B. Fabes, C. E. Kenig, and G. C. Verchota, *The Dirichlet problem for the Stokes system on Lipschitz domains*, Duke Math. J., 57 (1988), pp. 769–793.
11. C. Geuzaine and J.-F. Remacle, *Gmsh: A 3-D finite element mesh generator with built-in pre-and post-processing facilities*, International journal for numerical methods in engineering, 79 (2009), pp. 1309–1331.
12. P. Grisvard, *Problemes aux limites dans les polygones. mode d'emploi*, Bulletin de la Direction des Etudes et Recherches Series C Mathematiques, Informatique, 1 (1986), pp. 21–59.
13. D. Inzunza, F. Lepe, and G. Rivera, *Displacement-pseudostress formulation for the linear elasticity spectral problem*, Numer. Methods Partial Differential Equations, 39 (2023), pp. 1996–2017.
14. A. Khan, C. E. Powell, and D. J. Silvester, *Robust a posteriori error estimators for mixed approximation of nearly incompressible elasticity*, Internat. J. Numer. Methods Engrg., 119 (2019), pp. 18–37.
15. E. Koelink, J. M. van Neerven, B. de Pagter, and G. Sweers, *Partial differential equations and functional analysis: the Philippe Clément festschrift*, vol. 168, Springer Science & Business Media, 2006.
16. F. Lepe, S. Meddahi, D. Mora, and R. Rodríguez, *Mixed discontinuous Galerkin approximation of the elasticity eigenproblem*, Numer. Math., 142 (2019), pp. 749–786.
17. F. Lepe, G. Rivera, and J. Vellojin, *Mixed methods for the velocity-pressure-pseudostress formulation of the Stokes eigenvalue problem*, SIAM J. Sci. Comput., 44 (2022), pp. A1358–A1380.
18. ———, *A posteriori analysis for a mixed FEM discretization of the linear elasticity spectral problem*, J. Sci. Comput., 93 (2022), pp. Paper No. 10, 25.
19. C. Lovadina, M. Lyly, and R. Stenberg, *A posteriori estimates for the Stokes eigenvalue problem*, Numer. Methods Partial Differential Equations, 25 (2009), pp. 244–257.
20. S. Meddahi, *Variational eigenvalue approximation of non-coercive operators with application to mixed formulations in elasticity*, SeMA J., 79 (2022), pp. 139–164.

21. ———, *A DG method for a stress formulation of the elasticity eigenproblem with strongly imposed symmetry*, Comput. Math. Appl., 135 (2023), pp. 19–30.
22. S. Meddahi, D. Mora, and R. Rodríguez, *Finite element spectral analysis for the mixed formulation of the elasticity equations*, SIAM Journal on Numerical Analysis, 51 (2013), pp. 1041–1063.
23. R. Verfürth, *A posteriori error estimation techniques for finite element methods*, Numerical Mathematics and Scientific Computation, Oxford University Press, Oxford, 2013.
24. X. Zhong and W. Qiu, *Spectral analysis of a mixed method for linear elasticity*, SIAM Journal on Numerical Analysis, 61 (2023), pp. 1885–1917.